Article

Employing Conductive Metal-Organic Frameworks for Voltammetric Detection of Neurochemicals

Michael Ko, Lukasz Mendecki, Aileen M. Eagleton, Claudia G. Durbin, Robert M. Stolz, Zheng Meng, and Katherine A Mirica

J. Am. Chem. Soc., **Just Accepted Manuscript** • DOI: 10.1021/jacs.9b13402 • Publication Date (Web): 10 Mar 2020

Employing Conductive Metal−Organic Frameworks for Voltammetric Detection of Neurochemicals

Michael Ko,[1,†] Lukasz Mendecki,[1,†] Aileen M. Eagleton,[1] Claudia G. Durbin,[1] Robert M. Stolz,[1] Zheng Meng,[1] and Katherine A. Mirica*,[1]

[1]*Department of Chemistry, Burke Laboratory, Dartmouth College, Hanover, NH 03755*

ABSTRACT: This paper describes the first implementation of an array of two-dimensional (2D) layered conductive metal–organic frameworks (MOFs) as drop-casted film electrodes that facilitate voltammetric detection of redox active neurochemicals in a multianalyte solution. The device configuration comprises a glassy carbon electrode modified with a film of conductive MOF (M_3HXTP_2; M = Ni, Cu; and X = NH, 2,3,6,7,10,11-hexaiminotriphenylene (HITP) or O, 2,3,6,7,10,11-hexahydroxytriphenylene (HHTP)). The utility of 2D MOFs in voltammetric sensing is measured by the detection of ascorbic acid (AA), dopamine (DA), uric acid (UA), and serotonin (5-HT) in 0.1 M PBS (pH=7.4). In particular, Ni_3HHTP_2 MOF demonstrated nanomolar detection limits of 63 ± 11 nM for DA and 40 ± 17 nM for 5-HT through a wide concentration range (40 nM – 200 μM). The applicability in biologically-relevant detection was further demonstrated in simulated urine using Ni_3HHTP_2 MOFs for the detection of 5-HT with nanomolar detection limit of 63 ± 11 nM for 5-HT through a wide concentration range (63 nM – 200 μM) in the presence of constant background of DA. The implementation of conductive MOFs in voltammetric detection holds promise for further development of highly modular, sensitive, selective, and stable electroanalytical devices.

Introduction

Electrochemical detection of neurochemicals is an important tool for assessing stress and exertion, providing early diagnosis, treating disorders, and modifying human behavior.[1] Breakthroughs in designs of materials and devices have led to significant advances in rapid detection and continuous monitoring of neurochemicals in controlled environments.[2-8] Despite the sensitivity and selectivity of existing materials to a number of neurochemicals, three major challenges currently inhibit rapid progress toward technological applications. *First*, access to atomically-precise conductive nanomaterials with promising utility in electroanalysis (e.g., carbon nanotubes, graphene, metallic nanostructures, B-doped diamond) remains limited and costly.[9-12] *Second*, achieving desired sensitivity and selectivity with established materials typically requires additional post-synthetic chemical modification of the surface, often introducing extra processing steps that may generate surface defects, or yield composite materials with limited stability.[13-15] *Third*, integrating these nanomaterials into flexible, wearable, and biocompatible sensing devices poses challenges to chemical and mechanical stability of electrochemically-active interfaces within devices.[16] A conceptually novel technological approach that merges a unique class of chemically precise materials with three attributes including: 1) ease of synthetic access with no further chemical modifications, 2) high sensitivity and selectivity in multianalyte sensing, and 3) facile device integration with strong interfacial contact with the underlying substrate represents an unmet need in electroanalysis.

This paper describes the first systematic study for the implementation of two-dimensional (2D) conductive metal–organic frameworks (MOFs) as mediators in voltammetric detection of biologically-relevant analytes dopamine (DA), serotonin (5-HT), ascorbic acid (AA), and uric acid (UA)) in multianalyte aqueous solutions. These analytes are important due to the significant role of these molecules in human physiology, including mental, metabolic, and nutritional health.[17-20] Measuring the concentrations of DA and 5-HT provides an important approach for assessing stress and exertion, providing early diagnosis, treating disorders, and modifying human behavior.[1] DA is integral for motor control, cognition, reward, and motivation and endocrine functions.[21-23] Abnormal levels of DA can have serious consequences on health, implications in various diseases (e.g., depression, ADHD, schizophrenia, Parkinson's disease), and pheochromocytoma.[24-26] 5-HT is critical in the regulation of body temperature, appetite, sleep, memory, and mood.[24] The abundance of co-occurring electroactive species, AA and UA, commonly interfere with the detection of neurochemicals.[27] Parallel determination of these analytes through voltammetric measurements remains a challenge that has been addressed through extensive surface functionalization of established electrode materials.[28-29] Electrodes chemically modified electrodes with polymers,[30-37] enzymes,[38-43] ionic liquids,[44-48] or carbon coatings[49-55] have enabled detection of neurochemicals with nM–μM detection limits, however, the reliance on experimental design where analytical performance is manipulated through successive incorporation of multi-component electrocatalysts has several disadvantages. These disadvantages include reliance on composite materials with limited interfacial stability and lack of precise control over electrochemically active interfaces.[10, 27-28, 56-57]

In contrast to existing approaches based on post-synthetically modified or composite materials, we focused on the use of several structural analogs of layered 2D conductive MOFs that are constructed in a chemically-precise manner through coordination-driven self-assembly from molecular precursors. The MOFs comprise metallic nodes (Cu and Ni) interconnected with hexatopic triphenylene-based organic ligands (2,3,6,7,10,11-hexahydroxytriphenylene, HHTP and 2,3,6,7,10,11-hexaiminotriphenylene, HITP) that are arranged in the Kagome lattice (**Figure 1**).[58-59] Despite the wide range of applications of this class of materials in chemiresistive sensing of gases,[60-65] ion-to-electron transduction in potentiometry,[66] energy storage,[67-69] catalysis,[70-77] and electrochemically-driven reversible gas capture,[77] the use of conductive MOFs as active components in

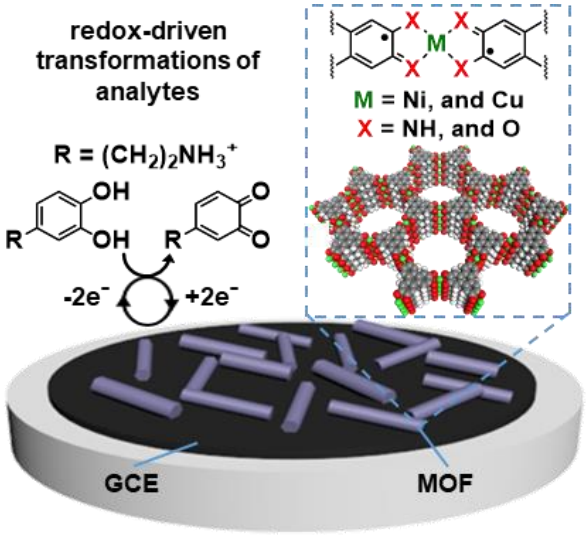

Figure 1. Schematic representation of the layered device architecture used in this study. A thin film of metal–organic framework (MOF) dispersed in H_2O is drop–casted directly on the top of a glassy carbon electrode (GCE) to enable voltammetric sensing of neurochemicals.

voltammetric detection of multianalyte systems have been limited.[78] To this day, MOFs have been primarily used as colorimetric sensors,[79-83] scaffolds,[84-86] and carriers[87-88] in biosensors rather than the electroactive materials due to limited conductivity and stability in aqueous solutions.[89] Recently, the ability to achieve conductivity in 3D MOFs, through doping or mixing with conductive materials such as carbon or metal nanoparticles, has enabled the implementation of these composite materials in the detection of glucose,[87] L-cystine,[90] and dopamine.[91] The drawbacks of doping and composite material use may result in the reduction of surface area, porosity, and pore volume as well as alter possible redox-active components embedded within the MOF leading to changes in the detection process.[59] Although a recent report has demonstrated the feasibility of using 2D MOFs for the electrochemical detection of dopamine, our report distinguishes itself by providing the first systematic investigation for using four structural analogs of water stable conductive MOFs for electrochemical detection of neurotransmitters, vitamins, and metabolites. [78]

Our strategy focuses on the design and studies of structure–property relationships of modular MOF-based layered film electrodes that can allow simultaneous detection of neurochemicals, while minimizing the interfering effects of other biologically-relevant analytes. Through a series of electrochemical measurements, we demonstrate that 2D conductive MOFs can be utilized as electrocatalysts for the detection of DA and 5-HT in the presence of important interferents, such as AA and UA in aqueous solutions. The MOFs in this study were able to simultaneously detect and resolve both DA and 5-HT and achieve single analyte limits of detection of 63 ± 11 nM and 40 ± 17 nM, respectively, while exhibiting electrochemical stability upon continuous cycling (at least 100 cycles). These performance characteristics rival the best-known electrochemical sensors for DA and 5-HT detection based on aptamers,[92-94] conductive polymer/carbon materials,[95-96] or β-cyclodextrin/graphene,[97] thus illustrating that this new generation of functional materials holds great potential for the development of selective and sensitive sensors. The modularity the MOF-based electrodes enables access to a sensing platform capable of targeted design of structure–property relationships for optimized detection of desired analytes.

Experimental Design

Advantages of conductive MOFs as working electrodes in electroanalysis. Our experimental design employs 2D porous conductive MOFs as modular film-based working electrodes (**Figure 1**). This class of material has at least three advantageous characteristics for broad implementation in electrochemical sensing. *First*, a large degree of structural control and compositional modularity can be achieved through bottom-up synthetic approaches,[58, 98] permitting the integration of known electrocatalytic components into the MOF (e.g., metallic nodes). *Second*, synthesized MOFs are permanently porous, with numerous potential active sites available for electrochemically-driven redox transformations.[68] This characteristic is important for obtaining large intensity of currents necessary for improving sensitivity of electrochemical sensors. *Third*, the class of MOFs based on the hexa-substituted triphenylene structures exhibits good electrical conductivity,[60, 99] thus potentially allowing for their direct implementation as working electrodes in analytical devices. We believe that these characteristics, when considered collectively, offer the possibility to develop conductive MOFs into versatile and integral components of electroanalytical devices with broad potential in chemical sensing.

The strategic choice of metal–organic frameworks. The molecular design in this study (**Figure 1, S1**) relies on the use of films of MOF-based electrodes comprising several conductive M_3HXTP_2 MOF analogs (M = Ni, Cu; X = NH, HITP or O, HHTP) differing in stacking patterns. This molecular design features metallic nodes (Ni, or Cu) with proven catalytic activity for redox-driven transformations of 5-HT, DA, AA, and UA and organic linkers that can engage in favorable intermolecular interactions with targeted molecules (e.g., electrostatic interactions or H-bonding).[40, 100-101] Several strategies have been utilized to optimize the electrode interaction to analytes, such as functionalization methods to promote adsorption,[9] introduction of dopants to alter electron transfer kinetics,[102] or coatings with polymers to increase selectivity.[103] Examples of optimized nanomaterials for improved electrochemical performance are, oxidation of graphene to increase adsorption of analytes onto the surface,[104] chemical modification of carbon nanotubes with oxygen containing (oxide, amide, and carboxylic acid) functional groups to promote analyte interactions with positively charged neurochemicals (DA and 5-HT),[105] incorporation of Cu/Ni nanoparticles or metal oxides to promote electrochemical activity,[33, 106-107] and coating negatively charged Nafion on polypyrrole-coated carbon fiber to discriminate against negatively charged species and increase the affinity for positively charged analytes such as dopamine.[108] We reasoned that designing electrode materials that constitute modified graphene analogs where atomic precision is controlled from the bottom-up may allow for modulation of MOF-analyte interactions to enable different degree of sensitivity and resolution in the detection of biologically important redox molecules.

Desirable characteristics of working electrodes for voltammetric detection of neurochemicals. There are several important design criteria for developing electrochemical sensors capable of detecting biomolecules.[109] *First*, the electrode should exhibit minimal to no intrinsic activity within the electrochemical measurement window of interest, such that it does not obscure electrochemical signals arising from the presence of the analytes.[110] *Second*, the electrode should exhibit tunable surface chemistry that can be readily optimized to ensure rapid and reversible electron transfer rates with surface-sensitive analytes.[109-110] *Third*, the electrode should exhibit reproducible electron transfer processes with resistance to fouling to enable continuous and repeatable detection of biologically-relevant analytes.[111] *Fourth*, the synthesis and material integration into devices should be sufficiently robust to produce excellent batch-to-batch reproducibility of devices with minimal conditioning and calibration requirements. The examination of several structurally analogous conductive MOFs as working electrodes, therefore, should allow optimization of these desirable characteristics through direct comparison of how the choice of chemical identity of the molecular precursors influences structure-property relationships of MOF-based working electrodes.

Strategic choice of analytes. In the study, we strategically chose specific inorganic and organic probes to demonstrate the capabilities of MOFs as working electrodes. We chose $Ru(NH_3)_6Cl_3$, $K_4Fe(CN)_6$, and $FeCl_3$ as the probes for two reasons. *First*, the selected inorganic probes have been widely utilized to characterize the electrochemical properties of new working electrodes, which allows for direct comparisons to existing working electrodes.[58, 61, 63, 112] *Second*, $K_4Fe(CN)_6$ and $FeCl_3$ are inner sphere redox probes that are typically surface sensitive, whereas $Ru(NH_3)_6Cl_3$ is an outer sphere redox probe that is typically surface insensitive.[113] These differences in electron transfer mechanisms thus directly probe the surface chemistry of the array of MOF-based working electrodes.[114] We also probed AA, DA, UA, and 5-HT as organic probes for three fundamental reasons. *First,* similar to the chosen inorganic probes, the selected organic probes are well characterized with a diverse set of working electrodes and electrolyte solutions allowing for a direct comparison in electroanalytical performance.[115-118] *Second*, the set of organic probes are important biochemical analytes that are critical to biological processes.[21-23] *Lastly*, we set out to overcome challenges that are observed with detection of AA, DA, UA, and 5-HT which include electrode fouling, irreversible redox processes, and the detection and resolution of all the analytes simultaneously.[119-124]

Results and Discussion

Synthesis and structural characterization of M_3HXTP_2 MOFs. We employed reticular synthesis through the reaction of hexatopic triphenylene-based linkers with divalent metal ions (M^{2+}) supplied in the form nickel (II) acetate, copper (II) sulfate, or copper (II) trifluoroacetylacetonate, to generate the corresponding M_3HXTP_2 MOFs: M_3(2,3,6,7,10,11-hexahydroxytriphenylene)$_2$ and M_3(2,3,6,7,10,11-hexaiminotriphenylene)$_2$ (M_3HHTP_2 and M_3HITP_2, respectively) where M = Ni, or Cu and X = NH, or O.[58, 60]

Powder X-ray diffraction patterns (pXRD) of M_3HXTP_2 (M = Ni, Cu; X = NH, O) matched reported characterization (**Figure S1**).[58, 60, 62, 65, 99] The pXRD traces obtained for M_3HXTP_2 indicated crystalline character with distinct diffraction peaks present at 2θ = 4.7, 12.6, 13.9, and 26.8 corresponding to the (100), (200), (3$\bar{1}$0) and (004) planes, respectively. (**Figure S1A**). All four simulated spectrums have very similar diffraction peaks present at 4.7, 12.6, and 26.8 degrees, but the intercalated peak present in Ni_3HHTP_2 leads to a diffraction peak around 13.9 degrees. **Figure S1B** clearly depicts the alternative stacking mode present in Ni_3HHTP_2 due to the intercalated layer which consists of metal-capped ligands.[58, 125]

Identity and morphology of the bulk MOFs were analyzed with scanning electron microscopy (SEM, **Figure 2**). Electron micrographs revealed the formation of randomly oriented MOF nanorods or globular structures in M_3HXTP_2 (M = Ni, Cu; and X = NH, O) (**Figure 2**). The bulk MOFs were further dispersed through sonication in H_2O to create suspensions of M_3HXTP_2 that aided in creating layered films (0.74 μm) when drop casted onto glassy carbon electrodes (GCE). PXRD analysis showed that the crystallinity of the

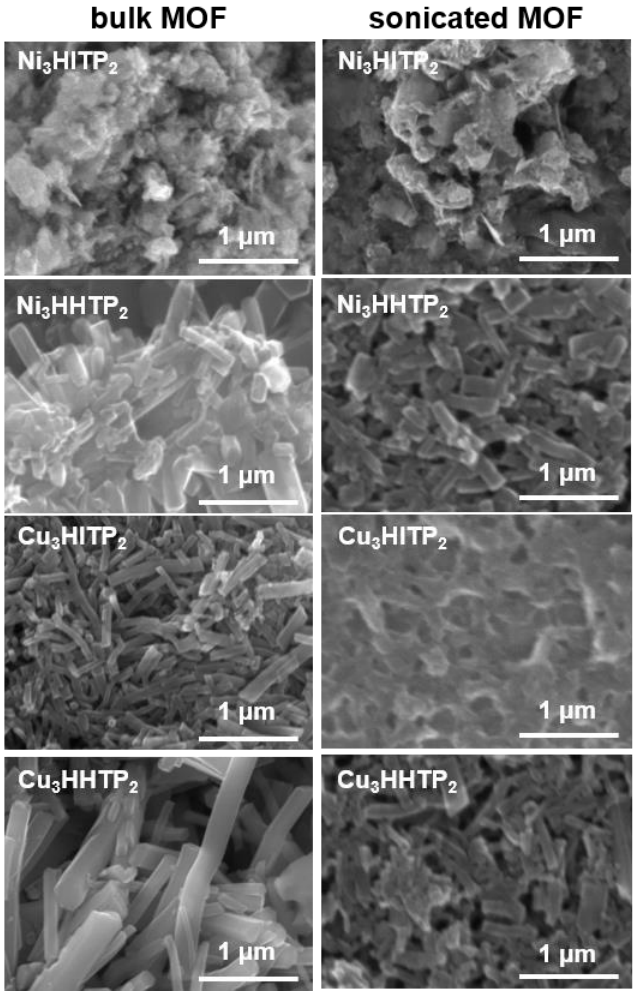

Figure 2. Scanning electron micrographs showing nanoscale morphology of M_3HXTP_2 MOFs (M = Ni, and Cu; X= NH, O) in bulk powder and after being dispersed in H_2O by sonication for 72 hours. All micrographs were taken at 50,000 x magnification and 7 mm working distance.

MOF dispersions was maintained after 72 hours of sonication (**Figure S2, S4**). SEM analysis of the drop-cast films on carbon tape confirmed that sonication did not substantially alter the crystallinity of the MOFs or the overall morphology (**Figure S3, S5**), but had a small influence on the particle size (**Figure 2**).

High resolution XPS spectra of Ni_3HHTP_2 and Ni_3HITP_2 MOFs revealed the presence of two distinct peaks with binding energies of ~851 and ~860 eV for Ni_3HXTP_2, which were assigned to 2p3/2 and 2p1/2 levels of Ni, respectively (**Figure S7, S8**).[72] Further deconvolution of Ni 2p regions confirmed that only one type of Ni^{2+} is present within Ni_3HXTP_2 MOFs (**Figure S7B and S8C**). Two distinct chemical environments were observed for Cu_3HXTP_2 MOFs with peaks maximum at approximately 932.8 and 934.6 eV, indicating mixed valency (Cu^{1+}/Cu^{2+}) within the framework (**Figure S9C and S10B**). These findings were consistent with previous reports.[60, 66]

The zeta potential for M_3HXTP_2 MOF suspensions were measured in 0.1 M PBS at pH =7.4. The total concentration of the MOF suspension measured was 0.1 mg in 1 mL of the PBS solution (**Table S1**). We observed zeta potentials between −20.9 mV and −27.8 mV indicating the MOF suspensions were negatively charged in the 0.1 M PBS solution at pH = 7.4. Zeta potentials less than −30 mV or greater than 30 mV are characterized as very stable suspensions.[126-127] Cu_3HHTP_2 had the most stable suspension with −27.8 mV and Ni_3HHTP_2 had the least stable suspension with −20.9 mV (**Table S1**).

Characterizing the intrinsic electrochemical properties of M_3HXTP_2 MOFs. The bulk electrical conductivity values for Ni_3HHTP_2, Ni_3HITP_2, Cu_3HHTP_2, and Cu_3HITP_2 have been previously measured and reported by us and others (2 S/cm – 2.0×10^{-2} S/cm).[60, 62-63, 99] To characterize applicability of MOF-based electrodes in voltammetric detection, we examined the intrinsic electrochemical performance of M_3HXTP_2 MOF layered films (M = Ni, Cu; and X = O, NH) drop-cast on GCE.

Voltammetric measurements such as cyclic voltammetry (CV) and differential pulse voltammetry (DPV) were conducted in 0.1M PBS specifically at pH=7.4 to emulate physiological conditions.[128-129] The CV of Ni_3HXTP_2 in 0.1 M PBS (pH = 7.4) drop-cast onto GCE revealed the presence of one slight anodic peak at −0.10 V and weak one cathodic redox wave at −0.24 V in Ni_3HHTP_2, indicating the presence of weak faradaic processes; no significant oxidation or reduction was observed for Ni_3HITP_2 (**Figure 3**). Cu_3HHTP_2 MOF in 0.1 M PBS exhibited a well-defined redox couple with two oxidation processes at −0.16 V and 0.13 V and one reduction process at −0.10 V. The voltammetric measurements of Cu_3HITP_2 MOFs had very similar redox couples to Cu_3HHTP_2 with two anodic peaks at −0.18 V and 0.11 V and one cathodic peak at −0.08 V (**Figure 3A**). In literature, similar cyclic voltammograms were observed in Cu complexes that attribute the observed two oxidation and two reduction peaks to a Cu^0 to Cu^{II} transitions.[130] In the case of Cu_3HHTP_2 and Cu_3HITP_2 MOFs in 0.1M PBS, we observed two oxidation peaks, but only one reduction peak which may indicate the lack of electrochemical reversibility or contributions from the redox non-innocent ligands. Both Cu-based MOFs exhibited a larger total charge from the oxidation process compared to the reduction process. The total charge of the combined oxidation process subtracted from reduction process were 7.1 C for Cu_3HHTP_2 and 2.0 C for Cu_3HITP_2. The difference is largely attributed to the first oxidation peak in the negative potential region that may suggest a large contribution from the redox active ligands HHTP and HITP, embedded in the Cu_3HHTP_2 and Cu_3HITP_2 MOFs respectively.[60, 60, 66]

PXRD and XPS data (**Figure S1 and Figure S7–S10**) confirmed that no metallic impurities or extraneous species were present within the frameworks of Cu_3HXTP_2 MOFs, while XPS revealed a mixed valent $Cu^{1+/2+}$ system. For the Ni_3HHTP_2 and Ni_3HITP_2 systems, XPS revealed only one redox state of Ni^{2+}, which may contribute to the limited redox activity observed by voltammetry (**Figure 3**). HHTP/HITP constituents may also undergo reversible redox transformations.[77, 131] We hypothesize that the observed distinct redox transitions for all studied M_3HXTP_2 MOFs may originate from the: i) redox activity of the metallic nodes or/and organic linkers;[132-134] ii) co-existence of several active redox states due to the presence of defects in

The observed electrochemical response is consistent with the studies of Ni_3HHTP_2 and Cu_3HHTP_2 MOFs by our group,[66, 77] and those of Dincă,[68] and Xu groups.[67] Specific differences in voltammetric response in different studies may be attributed to changes in experimental conditions including background electrolyte, ionic strength of the solution, electrode configuration, and the presence of additives. Given that MOFs exhibit permanent porosity, changes in the cumulative pore volume as a function of the MOF layer thickness deposited on the electrode surface may be further manifested by the unique voltammetry of these materials.[135]

Observation of electrochemical response of M_3HXTP_2 MOFs towards inorganic probes. Once the intrinsic electrochemical performance of these materials has been established, we examined the electrochemical response of 2D conductive MOFs to three inorganic redox probes including $Ru(NH_3)_6Cl_3$, $K_4Fe(CN)_6$, $FeCl_3$ in 0.1 M KCl (**Figure S12**). The electrochemical responses towards inorganic probes were influenced by the mechanism of electron transfer respective to each probe (**Figure S12**). The heterogeneous electron transfer for all M_3HXTP_2 MOFs was calculated using the Gileadi method[136] (**Figure S13 – S16**). The Gileadi method was used to calculate k_0, as opposed to the Nicholson method, as the calculations are not based on the observed peak which is limited to reversible systems but rather critical scan rate. We determined the critical scan rate by plotting the oxidation peak potential versus the log of the scan rate and observed two linear regions. The intersection between the slope of the low scan rate and high scan rate leads to the critical scan rate value.[136]

Ni_3HITP_2 exhibited the largest variation of heterogenous electron transfer rates with largest rates calculated for $Ru(NH_3)_6Cl_3$, followed by $K_3Fe(CN_6)$, and an irreversible redox process $FeCl_3$ (**Figure S12, Table 1**). Ni_3HHTP_2 followed the similar trend with the k_0 of $Ru(NH_3)_6Cl_3$ being the highest followed by $K_3Fe(CN_6)$, and lastly $FeCl_3$ exhibiting the lowest k_0 (**Figure S14, Table 1**). The same trend was observed with Cu_3HXTP_2 MOFs as the calculated heterogenous electron transfer rates were $Ru(NH_3)_6Cl_3$, $K_3Fe(CN_6)$,

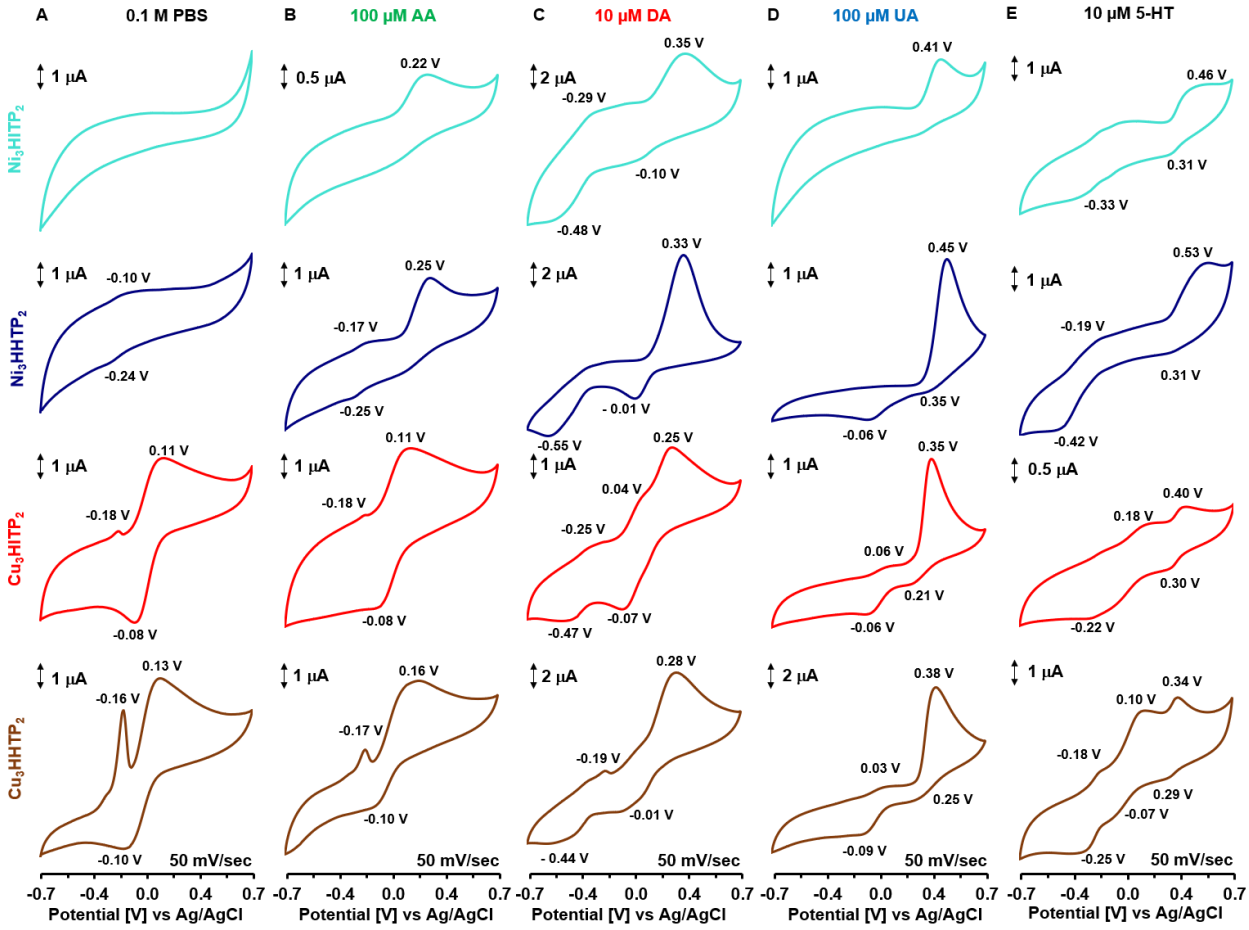

Figure 3. Cyclic voltammograms obtained for A) M_3HHTP_2 MOFs (M = Ni, and Cu) and M_3HITP_2 MOFs (M = Ni, and Cu) in 0.1 M PBS; B) 100 µM of AA; C) in 10 µM of DA; and D) in 100 µM of UA in 0.1 M PBS (pH = 7.4). All voltammetric measurements were run at 50 mV/sec using a three electrode configuration — MOF films coated glassy carbon electrode, silver/silver chloride, and platinum were used as working, reference, and counter electrodes, respectively. The solutions were degassed with N_2 prior to the electrochemical measurements and the drop-casted MOFs on the GCE electrode were initialized with 25 CV scans at 50 mV/sec.the MOF lattice (e.g., exposed-edges);[137] and iii) redox-active impurities that are permanently incorporated within the bulk of the porous framework, but are not observable by pXRD or XPS.

and $FeCl_3$ in order of largest to lowest. (**Figure S15, S16 and Table 1**). In general, the MOFs exhibited the fastest heterogenous electron transfer rates for $Ru(NH_3)_6Cl_3$ likely due to the surface insensitive nature of the inorganic probe.[113] The surface sensitive probes such as $K_4Fe(CN)_6$ and $FeCl_3$ exhibited a diverse range of heterogenous electron transfer rates. Generally, for the $K_4Fe(CN)_6$ inorganic probe, Ni_3HXTP_2 have larger k_0 values compared to Cu_3HXTP_2 MOFs. The reverse trend was observed for the $FeCl_3$ probe with no k_0 value for Ni_3HITP_2 and lower values for Ni_3HHTP_2 when compared to Cu_3HXTP_2 MOFs.[114] All the MOFs exhibited peak-to-peak separations of less than 70 mV for $Ru(NH_3)_6Cl_3$. In the case of $K_4Fe(CN)_6$, the peak separation ranged from 80 mV to 440 mV which was a semi-reversible response. All the MOFs exhibited minimal redox activity with the $FeCl_3$ inorganic probe leading no observable oxidation peak in the case of Ni_3HITP_2 or peak separations in the range of 240 mV to 310 mV (**Table S2**).

Overall, the surface chemistry of the MOFs, their packing morphology, and their intrinsic conductivity strongly influenced the electroanalytical response towards the three inorganic probes.[58, 61, 63, 112] The heterogenous electron transfer rates for the inorganic probes using MOFs were comparable to other electrode based systems. For example, multi-walled carbon nanotubes show k_0 of 3.67×10^{-3} cm s^{-1} for $K_4Fe(CN)_6$,[138-140] graphite electrodes show k_0 of 7.51×10^{-4} cm $s^{-1}$for $Ru(NH_3)_6Cl_3$,[139-141] and Pt disk electrodes show k_0 of 1.0×10^{-2} cm s^{-1} for $FeCl_3$.[142-143] The linearity observed in the lower scan rate Randles-Sevcik plots for scan rates 5–75 mV/s, (**Figure S13–S16**) show the electron transfer rates were diffusion driven. At higher scan rates from 100–1000 mV/s (**Figure S13–S16**), the MOFs exhibit less reversibility leading to slower heterogenous electron transfer rates (**Table 1**).

Observation of electrochemical response of M_3HXTP_2 MOFs towards biologically relevant probes. Figure 3 presents cyclic voltammetry for M_3HXTP_2 MOFs in the solutions containing AA (100 µM),[115] DA (10 µM),[116] UA (100 µM),[117] and 5-HT (10 µM)[118] at their clinically relevant concentrations, in 0.1 M PBS at pH = 7.4. Data exhibited oxidation and reduction peaks consistent with the analyte-centered redox activity, suggesting that the surface of the MOF functions as a mediator and/or electrocatalyst to promote the redox reactions for the specific analytes. The observed

Table 1. Heterogenous electron transfer rates obtained for M_3HXTP_2 MOFs (M = Ni, Cu; X = NH, O) in $Ru(NH_3)_6Cl_3$, $K_4Fe(CN_6)$, and $FeCl_3$.

	Ni_3HHTP_2 (cm s^{-1})	Ni_3HITP_2 (cm s^{-1})	Cu_3HHTP_2 (cm s^{-1})	Cu_3HITP_2 (cm s^{-1})
$Ru(NH_3)_6Cl_3$ (5–75 mV s^{-1})	5.12×10^{-3}	7.30×10^{-1}	2.36×10^{-2}	8.83×10^{-3}
$Ru(NH_3)_6Cl_3$ (100–1000 mV s^{-1})	6.41×10^{-3}	4.86×10^{-1}	2.36×10^{-2}	8.83×10^{-3}
$K_4Fe(CN)_6$ (5–75 mV s^{-1})	4.44×10^{-3}	5.42×10^{-3}	3.57×10^{-3}	3.72×10^{-2}
$K_4Fe(CN)_6$ (100–1000 mV s^{-1})	3.32×10^{-3}	5.42×10^{-3}	5.04×10^{-3}	1.78×10^{-2}
$FeCl_3$ (5–75 mV s^{-1})	9.05×10^{-4}	–	5.30×10^{-3}	2.38×10^{-3}
$FeCl_3$ (100–1000 mV s^{-1})	4.53×10^{-4}	–	1.30×10^{-3}	9.30×10^{-2}

similarities and differences in electrocatalytic activity towards biologically relevant probes (AA, DA, UA, and 5-HT) could be attributed to differences in chemical composition and structure (**Figure 3, S17**) of the analytes and MOFs. At physiological pH 7.4, AA is negatively charged,[120] UA neutral,[144] and DA[145] and 5-HT[146] are positively charged species; these characteristics may promote electrostatic interactions with the negatively charged MOF electrodes (**Table SI**). The extended π-framework of MOFs may also contribute to favorable interactions with aromatic structures in DA and 5-HT.[78]

Assessing the electrochemical response of M_3HXTP_2 MOFs towards ascorbic acid. The oxidation of AA is a two-electron, and one-proton mediated redox transformation, with electron-transfer kinetics being strongly influenced by the surface chemistry and microstructure of the electrode (**Scheme S1**).[119-122] The electrochemical oxidation of AA on unmodified surfaces (e.g., GCE) may result in the accumulation of reaction products on the electrode surface leading to irreversible voltammetric response.[119-122] Modifications to the electrode surface have been proposed to enhance electrode kinetics and improve reversibility of the system.[119-122] **Figure 3B, S3, S5, and S6** and **Table 2** demonstrate the voltammetric response obtained with MOF-coated electrodes for 100 μM of AA in 0.1 M PBS (pH = 7.4). Cu_3HXTP_2 MOFs showed no observable difference in oxidation peak potential between the MOF in 0.1 M PBS (pH=7.4) compared to the voltammetry in 100 μM AA (**Figure S22A–25A**), thus leading to inability to reliably detect AA. Voltammetric measurements of Ni_3HXTP_2 MOFs revealed irreversible response to cycling in the presence of AA, as evidenced by the presence of only an anodic peak. Applying the Gileadi method enabled the calculation of k_0 for the Ni_3HHTP_2 and Ni_3HITP_2 MOFs(**Table 2, Figure S18A–21A**). In the case of Ni_3HITP_2 at scan rates from 100–100 mV/s, the k_0 was not calculated due to the nonlinearity (R^2 of less than 0.91) in the trendline for the Randles-Sevcik plots (**Figure S19A**). The lower R^2 values can contribute to large deviations in calculations of the heterogenous electron transfer rates.

A difference between Ni_3HHTP_2, and Ni_3HITP_2 MOFs was a shift in anodic peak potential for AA ($E_{oxidation}$ = 0.25 V and 0.22 V, respectively), reflecting differences in surface sensitivity of AA oxidation (**Figure 3B**). Changes in voltammetric response between tested MOFs may be due to the differences in packing morphology of the MOFs (i.e., Ni_3HHTP_2 contains an interpolated layer that consists of a metal capped ligand layer in between the MOF framework layers)[58] or differences in pKa's of the capping substituents on the surface of the MOFs.

Probing the ability of MOF film modified electrodes to promote DA redox transformations. Voltammetry of DA is known to vary considerably on different electrode surfaces.[147] For instance, on the unmodified electrodes such as GCE, irreversible redox transformations lead to the formation of a passivating layer on the surface (**Scheme S2**).[123] In the case of graphitic electrodes, the response to DA is mainly dictated by the amount of edge site functionality which tends to enhance electron transfer rates, in contrast to materials where basal plane functionality dominates.[38] Higher loading of graphene-based materials on the electrode surface can also hinder the electron transfer rates due to the blockage of electroactive edges.[148] MOF modified electrodes in 10 μM of DA in 0.1 M PBS (pH = 7.4) (**Figure 3C**) demonstrated improved reversibility of the DA redox couple reactions over GCE@Nafion electrode.[149] The anodic peak potential in the range of 0.25 to 0.35 V for DA, and the appearance of a cathodic peak (**Figure 3C**, and **Table S2**) were observed. The electrodes coated with Ni_3HXTP_2 MOF displayed irreversible voltammetry as evidenced by the presence of broad redox peaks, large peak-to-peak separations of 340 mV and 450 mV. Cu_3HHTP_2 and Cu_3HITP_2 displayed semi-reversible characteristics indicated by the peak separations of 290 mV and 320 mV. The oxidation peaks of DA organic probe were observed in the Cu_3HXTP_2 MOFs system at 0.25 V (Cu_3HITP_2) and 0.28 V(Cu_3HHTP_2). In this case, the intrinsic redox activity of the Cu_3HXTP_2 MOFs (0.11 and 0.16 V) did not interfere with the anodic peak of DA (0.25 and 0.28 V).

The heterogenous electron transfer rates for DA were approximately an order of magnitude higher than observed for AA. Unlike the case of AA, all the MOFs presented a response which enabled the calculation of heterogenous electron transfer rates (**Table 2**). The Cu_3HITP_2 MOFs had the fastest k_0 followed by the Ni_3HXTP_2 MOFs, and lastly

Table 2. Heterogenous electron transfer rates obtained for M_3HXTP_2 MOFs (M = Ni, Cu; X = NH, O) in AA, UA, DA, and 5-HT.

	Ni_3HHTP_2 (cm s^{-1})	Ni_3HITP_2 (cm s^{-1})	Cu_3HHTP_2 (cm s^{-1})	Cu_3HITP_2 (cm s^{-1})
AA (5–75 mV s^{-1})	3.20×10^{-3}	1.64×10^{-4}	–	–
AA (100–1000 mV s^{-1})	5.43×10^{-3}	–	–	–
UA (5–75 mV s^{-1})	1.23×10^{-2}	2.92×10^{-3}	5.44×10^{-3}	2.59×10^{-2}
UA (100–1000 mV s^{-1})	–	–	5.88×10^{-3}	–
DA (5–75 mV s^{-1})	3.85×10^{-2}	2.63×10^{-2}	1.57×10^{-2}	6.25×10^{-2}
DA (100–1000 mV s^{-1})	2.25×10^{-2}	2.25×10^{-2}	1.41×10^{-2}	4.16×10^{-2}
5-HT (5–75 mV s^{-1})	3.23×10^{-2}	–	4.11×10^{-2}	1.41×10^{-2}
5-HT (100–1000 mV s^{-1})	–	–	8.75×10^{-2}	–

Cu_3HHTP_2 (**Figure S18B–25B**). The rates for all four MOFs were within the same order of magnitude with only a small difference between the lowest and highest values. The heterogenous electron transfer rates calculated using the scan rates 5–75 mV/s were faster than the 100–1000 mV/s. At lower scan rates, the interaction between DA and the MOFs were diffusion driven, but at faster scan rates the non-linear Randles-Sevcik plots show greater irreversibility thus slower heterogenous electron transfer rates. (**Figure S18B–25B**).

In graphitic electrodes, the enhanced redox activity towards DA oxidation is typically related to a higher degree of oxygen functionalities on the electrode surface. We hypothesized that the observed improvement in the response for different MOF film electrodes, compared to GCE, could be caused by three possible factors. *First*, the presence of attractive electrostatic interactions, hydrogen bonding, π-π interactions, or chelation between the MOF and DA may accelerate the electron transfer during oxidation, and thus give rise to enhanced voltammetric response. *Second*, a high degree of porosity of the studied MOFs may give a more sensitive response to DA than traditional macroelectrodes in which the mass transport occurs via semi-infinite diffusion. *Third*, the apparent differences in the catalytic effect to redox transformations between studied MOFs may suggest that the choice of node (Ni vs Cu) and the choice of heteroatomic crosslinker (NH vs O) contributes to the electroanalytical performance of MOF-based electrodes.

Measuring surface-sensitivity to uric acid oxidation. The oxidation of UA is typically irreversible at GCE and metal electrodes, and is quasi-reversible at graphite electrodes.[150-151] The electrochemical oxidation of UA undergoes two-electron and two-proton charge transfer typically resulting in the formation of an unstable di-imine species, which can be further converted into an imine-alcohol and then uric acid-4,5 diol (**Scheme S3**).[150] The uric acid-4,5 diol compound is largely unstable and can decompose to various side-products, depending on the solution pH, which may result in electrode fouling.[152]

To overcome the challenge with UA detection, we probed the redox activity of 100 μM UA in 0.1 M PBS (pH = 7.4) with cyclic voltammetry at MOF-modified electrodes. **Figure 3D** revealed that the drop-cast MOF-based layered films can successfully catalyze the oxidation of UA, with an overall reduction in the activation potential of almost 0.14 V, in the case of Cu_3HITP_2 toward the electro-negative region, in contrast to unmodified GCE (~0.49 V).[153-154] The oxidation peak maxima for Cu_3HXTP_2 (X= O, NH) MOF films were 0.38 V and 0.35 V respectively, but the Ni-analogs exhibited broad oxidation peak at 0.41 V and 0.45 V respectively (**Figure 3D**). All the MOFs, with the exception of Ni_3HITP_2, displayed a reversible process with peak separations of under 140 mV (**Table S2**). The voltammetric response of Ni_3HITP_2 may suggest slow electron transfer kinetics, potentially due to the fouling of the electrode surface by strongly adsorbed UA species.[152]

Of MOFs examined, electrodes modified with Ni_3HITP_2 demonstrated the slowest electron transfer kinetics, while Cu_3HITP_2 demonstrated the fastest electron transfer kinetics (**Table 2, Figure S18C–25C**). This observation suggests that the metal center may play a critical role for the kinetics of the MOFs. Interestingly in the case of the HHTP based MOFs, Ni_3HHTP_2 had slightly faster k_0 values compared to Cu_3HHTP_2. The slight difference may be attributed to the structural differences with Ni_3HHTP_2 containing the interpolated layer that is not present in Cu_3HHTP_2.[58] The linearity in the Randles-Sevcik plots at scan rates from 5–75 mV/s depict a diffusion driven process. At higher scan rates (100–1000 mV/s) the Randles-Sevcik plots displayed R^2 values of less than 0.91 which shows poor reversilibity, for Ni_3HHTP_2, Ni_3HITP_2, Cu_3HITP_2, therefore, the heterogenous electron transfer rates were not calculated for these MOFs (**Figure S18C–25C**).

The improved catalytic performance for UA oxidation over GCE observed for M_3HXTP_2 MOF (M = Ni, Cu; X = NH, O) modified electrodes may be due to the presence of surface-active sites, in the form of embedded metallic nodes or heteroatoms (NH, O) in the MOF framework. These sites can

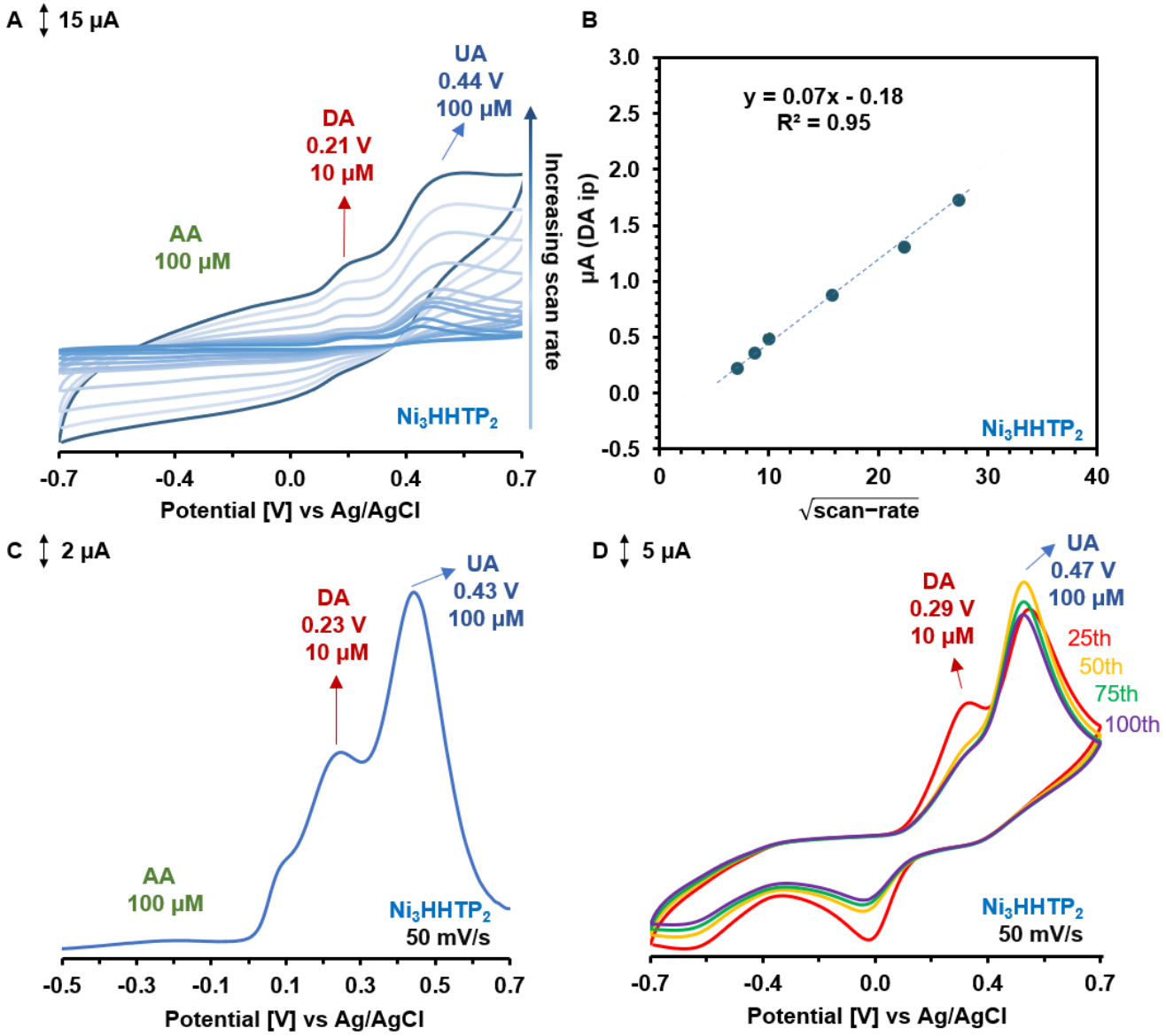

Figure 4. A) Cyclic voltammograms recorded for Ni_3HHTP_2 MOF in 100 µM of ascorbic acid, 100 µM of uric acid, and 10 µM of dopamine in 0.1 M PBS at different scan rates ranging from 5 mV/sec to 1000 mV/sec. B) Randles-Sevcik plot of the dopamine peak current vs. the √scan-rate. C) Differential pulse voltammetry recorded for MOFs in 100 µM of ascorbic acid, 100 µM of uric acid, and 10 µM of dopamine in 0.1 M PBS solution. D) Cyclic voltammetry showing representative scans at 25, 50, 75, 100th scan in 100 µM of ascorbic acid, 100 µM of uric acid, and 10 µM of dopamine in 0.1 M PBS solution DPV parameters: scan rate: 50 mV/sec; pulse width: 50 msec; and amplitude: 50 mV. The solutions were degassed with N_2 prior to the electrochemical measurements and the drop-casted MOFs on the GCE electrode were initialized with 25 CV scans at 50 mV/sec

potentially interact with UA through electrostatic interactions and/or hydrogen bonding or, leading to negative shift in their oxidation peak potential and peak current enhancements.

Probing the ability of MOF film modified electrodes to promote 5-HT redox transformations. On bare carbon based electrodes, the challenges in the detection of 5-HT results from oxidation products passivating the electrode surface leading to irreversibility, low sensitivity, and low selectivity.[118] To probe whether these issues could be overcome with MOF-based electrodes, we tested MOF-modified electrodes in 10 µM of 5-HT in 0.1 M PBS (pH = 7.4) (**Figure 3D**). All the materials examined in this study demonstrated improved cyclic voltammetric response of 5-HT compared to GCE electrodes. (**Figure S17**). The oxidation peak was observed in the window of 0.34 to 0.53 V for M_3HXTP_2 MOFs. Similar to DA, the oxidation potentials of 5-HT were lower for Cu_3HXTP_2 MOFs, ranging from 0.06–0.19 V, compared Ni_3HXTP_2 MOFs. The electrodes coated with Ni_3HHTP_2 and Ni_3HITP_2 MOFs displayed semi-reversible voltammetry with peak separations of 220 mV and 150 mV (**Figure 3E**). The electrodes modified with drop-cast layer of Cu_3HHTP_2 MOF exhibited a smaller peak-to-peak separation of 50 mV, where HITP analogs showed less reversible response with 100 mV peak separation (**Figure 3E**).

The observed heterogenous electron transfer rates were higher for the HHTP-based MOFs indicating that 5-HT demonstrated more favorable interactions with the HHTP containing materials. For the HITP based MOF electrodes, the k_0 could only be calculated for the Cu_3HITP_2 MOF, but not the Ni_3HITP_2 MOF (**Figure S18D–25D**) due to the R^2 values in the Randles-Sevcik plots calculated to be less than 0.91. The Randles-Sevcik plots using the scan rates from 5–75 mV/s shows a linear correlation meaning the electron transfer process was diffusion driven.

Detection of dopamine in the presence of interferants using voltammetry. After investigating voltammetric responses of M_3HXTP_2 MOFs to different redox probes (**Figure 3**, and **Table 2**), we focused on the detection of DA in the presence of common interferants (AA and UA) using Ni_3HHTP_2 MOF. We selected this MOF for three reasons: 1) it showed sufficiently reversible redox kinetics for the tested analytes; 2) it did not demonstrate strongly observable intrinsic redox activity that would obscure the detection of the selected analytes or interferants;[109-110] and 3) it maintained its morphology and crystallinity after sonication. Most importantly, the differences in redox potentials for DA and UA (0.33 V, and 0.47 V for Ni_3HHTP_2 MOF, respectively) make it possible to distinguish and quantify these analytes electrochemically in the same sample. In parallel to studying the electrochemical response of Ni_3HHTP_2, Ni_3HITP_2, Cu_3HITP_2, and Cu_3HHTP_2 MOFs were also studied in multi-analyte samples (**Figure S26–S29**). **Figure 4A** demonstrates cycling voltammograms recorded at different scan rates (5 mV/sec – 1000 mV/sec) in 0.1 M PBS solution containing a mixture of AA (100 μM), DA (10 μM), and UA (100 μM). The effect of the scan rate on the kinetics of charge transfer can be a useful parameter for controlling the intensities and the potentials of the redox waves (**Figure 4B**).

For each tested scan rate, the DA peak could be readily resolved from UA and AA (**Figure 4**). These findings can be explained by considering the selectivity of the oxidation of DA over the oxidation of AA. The observed limited detection of the oxidation of AA may arise from slow mass transfer of AA through the MOF framework and electrostatic repulsion between the negatively charged AA and negatively charged MOFs (**Figure 4A, Table S1**). The lack of noticeable response to AA does not pose a limitation towards the practical application of the Ni_3HHTP_2 functionalized electrode. On the contrary, it implies higher selectivity to other studied molecules including DA and UA, the detection of which is often compromised by the presence of the AA interferants.[155] The lack of electrochemical response to AA in turn, provides better resolution of DA (**Figure 4C**). Evaluation of long-term performance of Ni_3HHTP_2 MOF by examining the peak currents after continuous scanning showed an initial decrease in the peak intensity for oxidation current of DA at 0.29 V. After the initial decrease, the DA peak remained broadly unchanged up to 100 cycles (**Figure 4D**). The oxidation current of UA was retained up to >95% after 100 cycles demonstrating excellent stability (**Figure 4D**).

Quantitative determination of ascorbic acid, dopamine, uric acid, and serotonin using differential pulse voltammetry. In contrast to CV, DPV can offer significantly higher sensitivity for measured analytes at low concentrations due to minimal contribution of capacitive current to the measured signal.[156] Thus, to quantify the limit of detection and resolution of MOF-based sensors, we have assessed the electrochemical response of the glassy carbon electrodes modified with M_3HXTP_2 MOFs (M = Ni, Cu; X = NH, O) for the detection of AA, DA, UA, and 5-HT using DPV (**Figure S30–S34**). Specific concentrations of the analytes were predetermined to measure both the LOD and linear range of the MOF based sensors (**SI section IV C**). To provide a realistic representation of the detection capability of fabricated MOF-based sensors, all the reported detection limits were based on the lowest experimentally detectable concentrations where the analyte signal is visually and statistically distinct from the baseline using a calculation of signal-to-noise greater than three.

Figure 5 depicts the DPV recorded for Ni_3HHTP_2 in 0.1 M PBS with different concentrations of DA, and 5-HT. The experimental parameters were optimized based on the CV results with respect to best peak resolution and short scan time (scan rate: 50 mV/sec; pulse width: 50 mV; pulse amplitude: 50 msec) (**Figure 3**).

The DPV spectra recorded for each analyte (DA and 5-HT) exhibited a redox wave at a characteristic potential and the peak current that was dependent on the analyte concentration. As shown in **Figure 5A–B**, one strong anodic peak corresponding to the oxidation of DA and 5-HT were observed at 0.18 V and 0.30 V, respectively. The limit of detection for DA was 63 ± 11 nM and the magnitude of the oxidation peak currents recorded for DA increased linearly (63 nM–200 μM) with the concentration of the analyte (**Figure 5B)**. For 5-HT, the LOD was 40 ± 17 nM with two linear ranges of 20 nM – 10.0 μM and 20.0 μM – 200.0 μM.

Overall, out of the 4 different MOFs studied, Ni_3HHTP_2 did not exhibit an interfering oxidation peak inherent to the redox activity of the material and measured the lowest LOD values for the analytes of interest. Control electrodes were tested using unmodified GCE electrodes and then evaluated their electrochemical response to DA and 5-HT. The resulting unmodified GCE electrodes exhibited approximately 36 and 11 times higher detection limits for DA (2.31 ± 0.79 μM) and 5-HT (0.45 ± 0.17 μM) respectively (**Figure S34**) and significantly diminished peak current intensity than the Ni_3HHTP_2 (63 ± 11 nM and 40 ± 17 nM, respectively). These findings demonstrate that the presence of MOF can provide high sensitivity for DA determination at physiologically relevant levels (nM–μM).[38, 157-161]

Simultaneous detection of DA and 5-HT. We proceeded to probe the ability of MOF materials for simultaneous determination of 5-HT and DA due to the co-existence of these redox active analytes in many biological systems.[162] DPV of Ni_3HHTP_2 in 0.1 M PBS (pH = 7.4) revealed the ability to resolve and successfully differentiate between DA at 10 μM and 5-HT at 5 μM (**Figure 5C**). Using Ni_3HHTP_2 as the electrode, we observed two linear ranges of response: i) 70 nM–3.0 μM, and ii) 10.0 μM–200.0 μM with LOD for 5-HT of 92 ± 50 nM in the presence of 10 μM DA (**Figure 5D**). These observations suggest that Ni_3HHTP_2 MOF interacts strongly with 5-HT.

The reported DPV data (**Figure 5, S30–S34, and S41**) demonstrates that sensitivity and selectivity of MOF electrodes towards small molecule analytes could be modulated

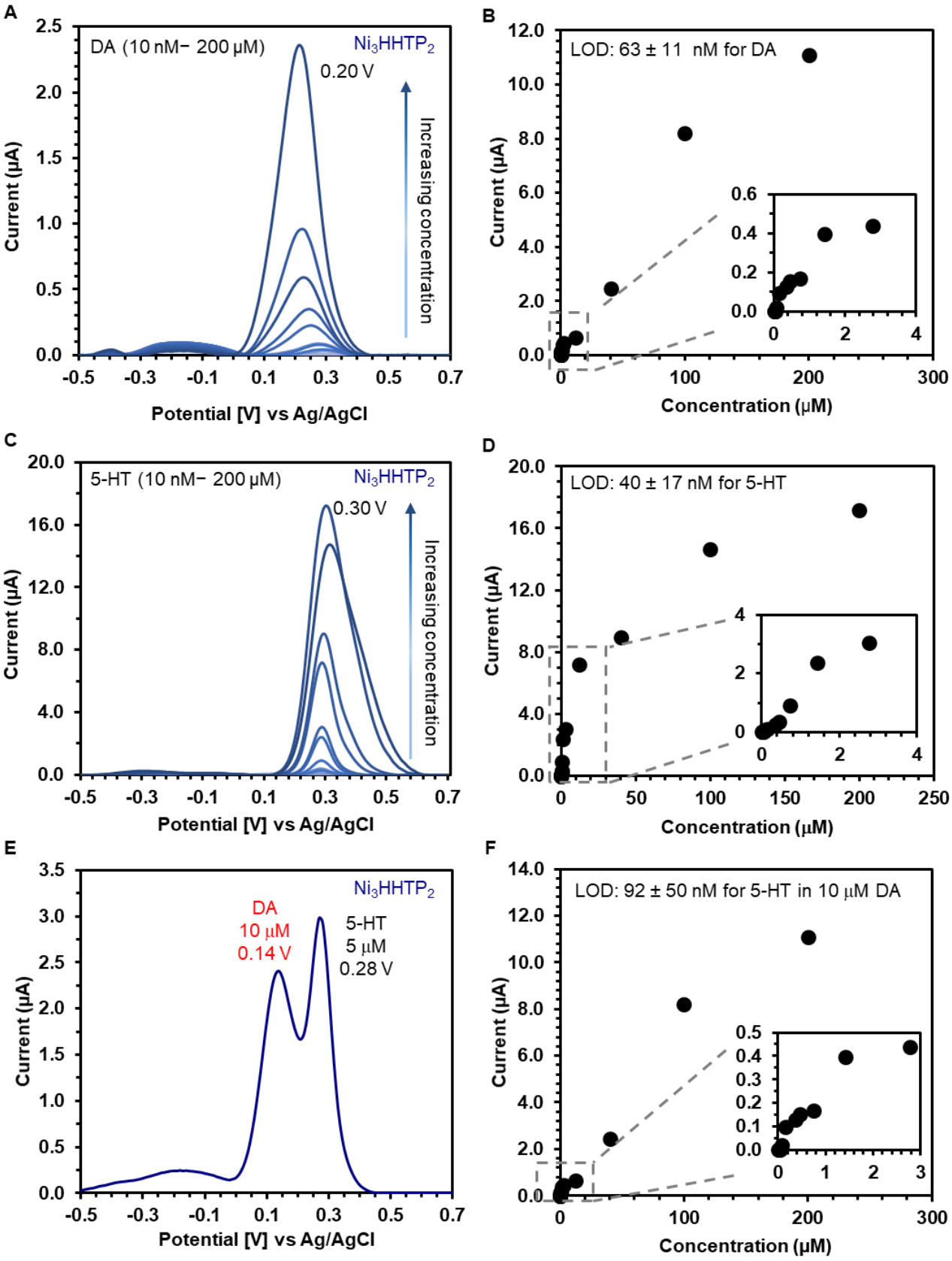

Figure 5. Differential pulse voltammograms recorded at varying concentrations of A) DA, B) the corresponding concentration dependence graph for DA, C) 5-HT, and D) the corresponding concentration dependence graph for 5-HT in 0.1 M PBS solution using Ni_3HHTP_2 coated glassy carbon electrode. E) Differential pulse voltammetry showing peak resolution between 10 µM DA and 5 µM 5-HT. F) Corresponding concentration dependence graph for 5-HT detection in the presence of 10 µM DA. DPV parameters: scan rate: 50 mV/sec; pulse width: 50 msec; and amplitude: 50 mV.

by altering the identity of the metallic node (Cu vs Ni) or the nature of the heteroatomic crosslinker within the MOF framework. For instance, tunable selectivity of conductive MOFs for DA or 5-HT oxidation may be achieved through varying the type of heteroatoms (e.g. X = NH, O) within the framework, which can exhibit different affinity for hydrogen-bonding formation between each analyte and the MOF.

Such degree of tunability could potentially allow the development of multi-electrode-based assays for simultaneous determination of biologically relevant molecules with no cross–reactivity and high sensitivity.

Evaluating batch-to-batch reproducibility and stability of M_3HHTP_2 MOF electrodes to electrochemical cycling, shelf-life, and reusability. The stability and reproducibility of the electrochemical sensors for the detection of biologically relevant analytes are an important criterion for device efficacy. The synthesis and device to device reproducibility for the detection of AA, DA and UA was measured using the oxidation potential of each respective analyte resulting in less than a 0.04 V difference between three different trials (**Figure S35**). Independent devices prepared through drop-casting 5 μL of Cu_3HHTP_2 MOF onto GCE demonstrated a consistent analytical response to 10 μM DA and 100 μM UA including the magnitude of current output peak position of targeted analytes (**Figure S35**). The electrodes drop-casted with two independently synthesized batches of M_3HXTP_2 MOF (M= Ni, Cu; X=O) (**Figure S36**) showed similar peak position and the magnitude of current output peak position of DA. The difference in the current output (2-3 μA) between analyzed batches may be potentially caused by the presence of defects (e.g., exposed leading edges, such as open metal and ligand sites in the framework),[79, 163] variation in film thickness, and/or varying degree of edge- and basal-plane sites present in the material as reported for other 2D materials such as graphene,[10] black phosphorous, and transition metal dichalcogenides.[164] These findings suggest that the electrodes prepared using different batches of the active material would require calibration.[157]

The repeatability of the MOF-based electrodes was assessed through subsequent exposures of the Ni_3HHTP_2 MOF to the solution containing DA, AA, and UA (**Figure S36**). We observed minimal deviation in the recorded peak current intensity after multiple sensing events (n=3) demonstrating good repeatability of the sensor for electrochemical measurements. Long-term stability of the MOF-based sensors was also evaluated using two tests. *First*, Ni_3HHTP_2 MOF suspension was stored for eight months at room temperature and *second*, the Ni_3HHTP_2 drop-casted film was exposed to air for two weeks on the GCE prior to performing DA detection (**Figure S38, S39**). The performance of the MOF modified GCE sensors was not significantly altered by prolonged storage conditions; these sensors still maintained high linearity (50 nM–3 μM; 3 μM–16 μM) and exhibited low detection limits (50–70 nM) to DA (**Figure 5, S35–S38**).

We also attempted to evaluate the structural stability of MOF-modified electrodes to electrochemical cycling by performing dopamine sensing, and subsequently analyzing the same material with PXRD. Unfortunately, small quantities of MOF used as films in voltammetric detection (5.0 μg) were not sufficient to produce a diffraction pattern. However, we were able to assess the stability of the MOFs after electrochemical analysis through SEM analysis (**Figure S40**). SEM analysis revealed that Ni_3HHTP_2 MOFs maintained their nanorod morphology even after cyclic voltammetry measurements (25 scans) in 10 μM DA and 5-HT. These findings indicate that the GCE modified with the drop-cast layer of conductive MOF are promising candidates as working electrodes for electroanalysis of biomedically-relevant analytes.

Detection of dopamine and serotonin in simulated urine. The implementation of conductive 2D MOFs in clinical applications may have potential utility for disease diagnostics[165] and monitoring of drug delivery[166]. The elevated levels of DA (420nM–2μM) or 5-HT (>1.6μM) in the urine may implicate pheochromocytoma tumors[165] or carcinoid tumors,[167] respectively. The monitoring of DA and 5-HT is also a powerful tool for ensuring the appropriate dosages of drugs are delivered to patients for the treatment and management of Parkinson's disease[168] and depression.[166]

The electroactive materials were tested in simulated urine for two reasons. *First*, to gain a perspective on the potential for the MOFs to be utilized for biological analysis, the electrochemical analysis needs to be conducted in stable and controlled concentrations.[169] Samples of human urine may vary from person to person due to differences in time of day, activity level, and diet before urine sample collection.[169] *Second*, a standard calibration curve is often generated in simulated urine to compare against the readings in urine samples, and thus forms the starting point for electroanalytical applications.[170-171] Simulated urine was prepared according to established procedures (major chemical species include 170 mM urea, 90 mM sodium chloride, and 25 mM ammonium chloride.[171]

As a preliminary demonstration of biological applicability, we investigated the ability of Ni_3HHTP_2 for the detection of DA and 5-HT DPV in simulated urine (**Figure S41**).[169, 171 172-173] We observed that the LOD for DA in simulated urine was higher at 416 ± 57 nM compared to the LOD in 0.1 M PBS (63 ± 11 nM) (**Figure S41B**). The LOD of 5-HT in simulated urine was 63 ± 11 nM, which is comparable to the LOD in 0.1M PBS (40 ± 17 nM) (**Figure S41D**). The ability of Ni_3HHTP_2 to oxidize 5-HT was not hindered by the additional chemical species in simulated urine or the change in pH. The resolution for distinct peaks corresponding to the oxidation of DA (10 μM) and 5-HT (5 μM) was maintained in simulated urine (**Figure S41E**). Detection of 5-HT in the presence of DA (10 μM) in simulated urine using DPV revealed a LOD of 420 ± 50 nM for 5-HT.

The change in pH from 7.4 in 0.1 M PBS to 6.0 in simulated urine can also affect the interaction between the target analytes (DA and 5-HT) and the MOF. Many literature studies show pH dependence of peak current for DA (pH= 6, highest cathodic peak current) and 5-HT (pH=7, highest cathodic peak current). The LOD studies are conducted in the specified pH for the greatest detection of the analyte The increase in pH also leads to a gradual shift from positive to negative peak potentials and change in peak separations of DA and 5-HT observed through cyclic voltammetry.[96, 174-176] Future studies that rely on pH-dependent resolution of analytes may further improve the detection of neurochemicals in body fluids.[36, 177-178]

CONCLUSIONS

This work describes the systematic investigation of 2D conductive metal–organic frameworks as efficient electrocatalysts to achieve electrochemical detection of DA, 5-HT, AA, and UA in aqueous solutions. Based on this study, we identify at least four fundamental advances for the development of MOF-based electrochemical sensors for neurochemical detection. *First*, the electroanalytical response (e.g., electron transfer rate or sensitivity) of conductive 2D MOFs to AA, DA, UA, and 5-HT can be modulated by tuning the MOF chemical structure. The identity of the metal and ligand within the MOF strongly influences the kinetics of heterogeneous electron transfer. For the biologically relevant analytes (AA, DA, UA, and 5-HT) Ni_3HHTP_2 MOF generally had the most efficient heterogenous electron transfer rates, compared to the rest of the MOFs. In the HHTP ligand-based MOFs, Ni_3HHTP_2 usually demonstrated higher heterogenous electron transfer rates for most probes, compared to Cu_3HHTP_2 based MOFs. The heterogenous electron transfer rates of M_3HXTP_2 MOFs for DA (k_0 = 3.85 × 10^{-2} cm s^{-1} Ni_3HHTP_2, 2.63 × 10^{-2} cm s^{-1} Ni_3HITP_2, 1.57 × 10^{-2} cm s^{-1} Cu_3HHTP_2, 6.25 × 10^{-2} cm s^{-1} Cu_3HITP_2) are in between sensors based on GCE modified with multiwalled carbon nanotubes and cobalt phthalocyanine nanocomposite (5.40 × 10^{-4} cm s^{-1})[122] or pure GCE (3.6 × 10^{-1} cm s^{-1}).[123] *Second*, MOF-modified electrodes exhibited excellent analyte sensitivity with nanomolar detection limits (Ni_3HHTP_2: DA = 63 nM ± 11 nM, and 5-HT = 40 nM ± 17 nM) and good signal resolution. The sensing results for dopamine surpass the performance of electrodes based on other nanostructured materials, including graphene (2.6 μM),[38] graphene nanoflakes (1–10 μM),[157] carbon fiber (1 μM),[158] graphene oxide (0.27 μM),[159] 2D hexagonal boron nitride (0.65 μM),[160] and 3D carbon nanotube nanoweb (1–20 μM).[161] The sensing response for serotonin compares to materials including reduced graphene oxide/polyaniline (11.7 nM)[179], WO_3 nanoparticles (1.42 nM),[180] multilayered molecularly imprinted polymers (100 nM),[181] and poly(bromocresol green (80 nM).[182] Although the sensitivity of our devices does not yet exceed the best LOD reported for dopamine or serotonin detection obtained using highly optimized materials with integrated aptamer-functionalized graphene/polymer composite (0.002 nM for DA)[92] and electropolymerized film of 3-amino-5-mercapto-1,2,4-triazole on glassy carbon (0.013 nM for 5-HT)[183], the simplicity of accessibility of isoreticular MOF analogs through bottom-up solution chemistry offers a potential advantage. *Third*, MOF-based voltage-actuated sensors described herein demonstrate the important role in the modularity of the MOFs leading to analyte specific stability to electrochemical cycling and that their analytical response to tested neurochemicals is minimally compromised by the adsorption and subsequently passivation of electrode surface as observed for unmodified GCE[123] or metal–based electrodes.[6] *Fourth*, in contrast to many carbon-based electrodes, we observed small variability in the analytical response shown through the batch-to-batch reproducibility studies. Current fabrication methods for carbon-based materials offer limited control over the presence of impurities and defects that significantly can alter the electroanalytical performance of resulting sensors.[148, 184]

Despite the promise of 2D conductive MOFs in biosensing applications, the current implementation of M_3HXTP_2 MOFs (M = Ni, Cu; X = NH, O) in voltammetric sensing of neurotransmitters has three limitations: *First*, the morphological control over conductive MOF-based nanostructures has not yet been optimized. This lack of control limits the fundamental investigation of the roles of leading edges and basal planes play in electroanalysis. Continued efforts in synthetic optimization of morphological control over MOF-based nanomaterials[62, 65-66] and their structural defects[64, 185] will be critical to fundamental understanding the electroanalytical performance of conductive MOFs. *Second*, this study focuses on the use of semiconductive MOF materials with electrical conductivity ranging from 2.0×10^{-2} to 2 S cm^{-1}.[99] This semiconductive nature limits the electron transfer rates, thus potentially limiting the overall performance of electrochemical analysis. The design and synthesis of new MOFs based on highly conducting metal–ligand combinations, and ability to obtain monolayers or single crystals of conductive MOFs that resist opening of the band gap due to junctions between crystallites,[186] may overcome issues with limited electronic conductivity. *Third,* this work focuses on proof-of-concept detection of DA, 5-HT, AA, and UA, under controlled conditions, in phosphate-buffered saline and simulated urine rather than in clinical samples. The heterogenous electron transfer rates can be greatly influenced by the pH of the solvent and presence of competing interferents. Thus, further optimization of the MOF-based electrodes may be needed for the detection of analytes in complex urine and human serum samples. We anticipate that, with further development, the findings of this first proof-of-concept study will open new avenues for implementing conductive 2D MOFs as broadly applicable components in biologically relevant electroanalysis.[58-59, 61]

We expect that the experimental approach described herein may advance the field of electrochemical sensors. Because metal–organic frameworks are so broadly applicable and synthetically accessible, we anticipate that their application in electroanalysis for the determination of biologically-relevant species can be further tuned and adapted to produce multifunctional, and stable electrochemical sensing devices. Ultimately, strategies for the implementation and integration of conductive MOFs into selective and sensitive microelectrode arrays may offer promising opportunities for spatiotemporal assessment of neurochemicals in biological systems.[187-191]

ASSOCIATED CONTENT

Supporting Information. Experimental details, voltammetric data, scanning electron microscopy (SEM), energy-dispersive X-ray spectroscopy, X-ray photoelectron spectra. This material is available free of charge via the Internet at http://pubs.acs.org.

AUTHOR INFORMATION

Corresponding Author

*katherine.a.mirica@dartmouth.edu

Present Addresses

Burke Laboratory, 41 College Street, Dartmouth College, Hanover, NH, USA.

Author Contributions

†These authors contributed equally to this work.

The manuscript was written through contributions of all authors. All authors have given approval to the final version of the manuscript.

ACKNOWLEDGMENT

The authors acknowledge support from start-up funds provided by Dartmouth College, from Walter and Constance Burke Research Initiation Award, from National Science Foundation EPSCoR award (#1757371), the Army Research Office Young Investigator Program Grant No. W911NF-17-1-0398, Sloan Research Fellowship (#26019), Cottrell Scholar Award (#26019), 3M Non-Tenured Faculty Award, and James O. Freedman Presidential Scholars Program. The authors thank the University Instrumentation Center at the University of New Hampshire (Durham, NH) for access to the XPS and SEM.

REFERENCES

1. Schultz, W.; Dayan, P.; Montague, P. R., A Neural Substrate of Prediction and Reward. *Science* **1997,** *275*, 1593-1599.
2. Wightman, R. M., Probing Cellular Chemistry in Biological Systems with Microelectrodes. *Science* **2006,** *311*, 1570-1574.
3. Privett, B. J.; Shin, J. H.; Schoenfisch, M. H., Electrochemical Nitric Oxide Sensors for Physiological Measurements. *Chem. Soc. Rev.* **2010,** *39*, 1925.
4. Malinski, T.; Taha, Z., Nitric Oxide Release from a Single Cell Measured in situ by a Porphyrinic-Based Microsensor. *Nature* **1992,** *358*, 676-678.
5. Kruss, S.; Landry, M. P.; Vander Ende, E.; Lima, B. M. A.; Reuel, N. F.; Zhang, J.; Nelson, J.; Mu, B.; Hilmer, A.; Strano, M., Neurotransmitter Detection using Corona Phase Molecular Recognition on Fluorescent Single-Walled Carbon Nanotube Sensors. *J. Am. Chem. Soc.* **2014,** *136*, 713-724.
6. Robinson, D. L.; Hermans, A.; Seipel, A. T.; Wightman, R. M., Monitoring Rapid Chemical Communication in the Brain. *Chem. Rev.* **2008,** *108*, 2554-2584.
7. Li, B.-R.; Hsieh, Y.-J.; Chen, Y.-X.; Chung, Y.-T.; Pan, C.-Y.; Chen, Y.-T., An Ultrasensitive Nanowire-Transistor Biosensor for Detecting Dopamine Release from Living PC12 Cells under Hypoxic Stimulation. *J. Am. Chem. Soc.* **2013,** *135*, 16034-16037.
8. Alivisatos, A. P.; Andrews, A. M.; Boyden, E. S.; Chun, M.; Church, G. M.; Deisseroth, K.; Donoghue, J. P.; Fraser, S. E.; Lippincott-Schwartz, J.; Looger, L. L.; Masmanidis, S.; McEuen, P. L.; Nurmikko, A. V.; Park, H.; Peterka, D. S.; Reid, C.; Roukes, M. L.; Scherer, A.; Schnitzer, M.; Sejnowski, T. J.; Shepard, K. L.; Tsao, D.; Turrigiano, G.; Weiss, P. S.; Xu, C.; Yuste, R.; Zhuang, X., Nanotools for Neuroscience and Brain Activity Mapping. *ACS Nano* **2013,** *7*, 1850-1866.
9. McCreery, R. L., Advanced Carbon Electrode Materials for Molecular Electrochemistry. *Chem. Rev.* **2008,** *108*, 2646-2687.
10. Chandran, G. T.; Li, X.; Ogata, A.; Penner, R. M., Electrically Transduced Sensors Based on Nanomaterials. *Anal. Chem.* **2017,** *89*, 249-275.
11. Koppang, M. D.; Witek, M.; Blau, J.; Swain, G. M., Electrochemical Oxidation of Polyamines at Diamond Thin-Film Electrodes. *Anal. Chem.* **1999,** *71*, 1188-1195.
12. Swain, G. M.; Ramesham, R., The Electrochemical Activity of Boron-Doped Polycrystalline Diamond Thin Film Electrodes. *Anal. Chem.* **1993,** *65*, 345-351.
13. Yang, W.; Ratinac, K. R.; Ringer, S. P.; Thordarson, P.; Gooding, J. J.; Braet, F., Carbon Nanomaterials in Biosensors: Should You Use Nanotubes or Graphene? *Angew. Chem., Int. Ed.* **2010,** *49*, 2114-2138.
14. Salavagione, H. J.; Díez-Pascual, A. M.; Lázaro, E.; Vera, S.; Gómez-Fatou, M. A., Chemical Sensors Based on Polymer Composites with Carbon Nanotubes and Graphene: the Role of the Polymer. *J. Mater. Chem. A* **2014,** *2*, 14289-14328.
15. Sajid, M.; Nazal, M. K.; Mansha, M.; Alsharaa, A.; Jillani, S. M. S.; Basheer, C., Chemically Modified Electrodes for Electrochemical Detection of Dopamine in the Presence of Uric Acid and Ascorbic Acid: A Review. *Trends Anal. Chem.* **2016,** *76*, 15-29.
16. Bandodkar, A. J.; Jeerapan, I.; Wang, J., Wearable Chemical Sensors: Present Challenges and Future Prospects. *ACS Sensors* **2016,** *1*, 464-482.
17. Ames, B. N.; Cathcart, R.; Schwiers, E.; Hochstein, P., Uric Acid Provides an Antioxidant Defense in Humans Against Oxidant- and Radical-Caused Aging and Cancer: a Hypothesis. *Proc. Natl. Acad. Sci. U.S.A.* **1981,** *78*, 6858-6862.
18. Michael, D. J.; Wightman, R. M., Electrochemical Monitoring of Biogenic Amine Neurotransmission in Real Time. *J. Pharm. Biomed. Anal.* **1999,** *19*, 33-46.
19. Cooper, J. R.; Bloom, F. E., *The Biochemical Basis of Neuropharmacology*. 7th ed ed.; Oxford University Press: New York, 1996;
20. Rice, M. E., Ascorbate Regulation and its Neuroprotective Role in the Brain. *Trends Neurosci.* **2000,** *23*, 209-216.
21. Beninger, R. J., The Role of Dopamine in Locomotor Activity and Learning. *Brain Res. Rev.* **1983,** *6*, 173-196.
22. Berridge, K. C.; Robinson, T. E., What is the Role of Dopamine in Reward: Hedonic Impact, Reward Learning, or Incentive Salience? *Brain Res. Rev.* **1998,** *28*, 309-369.
23. Pivonello, R.; Ferone, D.; Lombardi, G.; Colao, A.; Lamberts, S. W.; Hofland, L. J., Novel Insights in Dopamine Receptor Physiology. *Eur. J. Endocrinol.* **2007,** *156*, 13-21.
24. Kundys-Siedlecka, M.; Baczynska, E.; Jonsson-Niedziolka, M., Electrochemical Detection of Dopamine and Serotonin in the Presence of Interferences in a Rotating Droplet System. *Anal. Chem.* **2019,** *91*, 10908-10913.
25. Lohr, K. M.; Masoud, S. T.; Salahpour, A.; Miller, G. W., Membrane Transporters as Mediators of Synaptic Dopamine Dynamics: Implications for Disease. *Eur. J. Neurosci.* **2017,** *45*, 20-33.
26. Feldman, J. M., Increased Dopamine Production in Patients with Carcinoid Tumors. *Metabolism* **1985,** *34*, 255-260.
27. Si, B.; Song, E., Recent Advances in the Detection of Neurotransmitters. *Chemosensors* **2018,** *6*, 1.
28. Bucher, E. S.; Wightman, R. M., Electrochemical Analysis of Neurotransmitters. *Annu. Rev. Anal. Chem.* **2015,** *8*, 239-261.

29. Jeon, J.; Hwang, I.; Chung, T. D., Electrochemical Detection of Neurotransmitters: Toward Synapse-Based Neural Interfaces. *Biomed. Eng. Lett.* **2016,** *6*, 123-133.
30. Ekinci, E.; Erdogdu, G.; Karagozler, A. E., Preparation, Optimization, and Voltammetric Characteristics of Poly(o-phenylenediamine) Film as a Dopamine-Selective Polymeric Membrane. *J. Appl. Polym. Sci.* **2001,** *79*, 327-332.
31. Gorle, D. B.; Kulandainathan, M. A., Electrochemical Sensing of Dopamine at the Surface of a Dopamine Grafted Graphene Oxide/Poly(methylene blue) Composite Modified Electrode. *RSC Adv.* **2016,** *6*, 19982-19991.
32. Fabregat, G.; Armelin, E.; Alemán, C., Selective Detection of Dopamine Combining Multilayers of Conducting Polymers with Gold Nanoparticles. *J. Phys. Chem. B* **2014,** *118*, 4669-4682.
33. Lakshmi, D.; Bossi, A.; Whitcombe, M. J.; Chianella, I.; Fowler, S. A.; Subrahmanyam, S.; Piletska, E. V.; Piletsky, S. A., Electrochemical Sensor for Catechol and Dopamine Based on a Catalytic Molecularly Imprinted Polymer-Conducting Polymer Hybrid Recognition Element. *Anal. Chem.* **2009,** *81*, 3576-3584.
34. Xue, C.; Han, Q.; Wang, Y.; Wu, J.; Wen, T.; Wang, R.; Hong, J.; Zhou, X.; Jiang, H., Amperometric Detection of Dopamine in Human Serumby Electrochemical Sensor Based on Gold Nanoparticles Doped Molecularly Imprinted Polymers. *Biosens. Bioelectron.* **2013,** *49*, 199-203.
35. Kumar, S. S.; Mathiyarasu, J.; Phani, K. L., Exploration of Synergism Between a Polymer Matrix and Gold Nanoparticles for Selective Determination of Dopamine. *J. Electroanal. Chem.* **2005,** *578*, 95-103.
36. Jin, G.; Zhang, Y.; Cheng, W., Poly(p-aminobenzene sulfonic acid)-Modified Glassy Carbon Electrode for Simultaneous Detection of Dopamine and Ascorbic Acid. *Sens. and Actu B. Chem.* **2005,** *107*, 528-534.
37. Zhang, R.; Jin, G.-D.; Chen, D.; Hu, X.-Y., Simultaneous Electrochemical Determination of Dopamine, Ascorbic Acid and Uric Acid using Poly(acid chrome blue K) Modified Glassy Carbon Electrode. *Sens. and Actu B. Chem.* **2009,** *138*, 174-181.
38. Njagi, J.; Chernov, M. M.; Leiter, J. C.; Andreescu, S., Amperometric Detection of Dopamine in Vivo with an Enzyme Based Carbon Fiber Microbiosensor. *Anal. Chem.* **2010,** *82*, 989-996.
39. Monica, F.; Melinda, D., Tyrosinase-Based Biosensors for Selective Dopamine Detection. *Sensors* **2017,** *17*, 1314.
40. Jackowska, K.; Krysinski, P., New Trends in the Electrochemical Sensing of Dopamine. *Anal. Bioanal. Chem.* **2013,** *405*, 3753-3771.
41. Özel, R. E.; Hayat, A.; Andreescu, S., Recent Developments in Electrochemical Sensors for the Detection of Neurotransmitters for Applications in Biomedicine. *Anal. Lett.* **2015,** *48*, 1044-1069.
42. Mangombo, Z. A.; Key, D.; Iwuoha, E. I.; Baker, P. G. L., Development of L-Phenylalanine Biosensor and its Application in the Real Samples. *Insciences J.* **2013,** 1-23.
43. Rahman, S. F.; Min, K.; Park, S.-H.; Park, J.-H.; Yoo, J. C.; Park, D.-H., Selective Determination of Dopamine with an Amperometric Biosensor using Electrochemically Pretreated and Activated Carbon/Tyrosinase/Nafion®-Modified Glassy Carbon Electrode. *Biotechnol. Bioprocess Eng.* **2016,** *21*, 627-633.
44. Cosnier, S.; Innocent, C.; Allien, L.; Poitry, S.; Tsacopoulos, M., An Electrochemical Method for Making Enzyme Microsensors. Application to the Detection of Dopamine and Glutamate. *Anal. Chem.* **1997,** *69*, 968-971.
45. Zhu, Z.; Qu, L.; Guo, Y.; Zeng, Y.; Sun, W.; Huang, X., Electrochemical Detection of Dopamine on a Ni/Al Layered Double Hydroxide Modified Carbon Ionic Liquid Electrode. *Sens. and Actu B. Chem.* **2010,** *151*, 146-152.
46. Zhao, Y.; Gao, Y.; Zhan, D.; Liu, H.; Zhao, Q.; Kou, Y.; Shao, Y.; Li, M.; Zhuang, Q.; Zhu, Z., Selective Detection of Dopamine in the Presence of Ascorbic Acid and Uric Acid by a Carbon Nanotubes-Ionic Liquid Gel Modified Electrode. *Talanta* **2005,** *66*, 51-57.
47. Safavi, A.; Maleki, N.; Moradlou, O.; Tajabadi, F., Simultaneous Determination of Dopamine, Ascorbic Acid, and Uric Acid using Carbon Ionic Liquid Electrode. *Anal. Biochem.* **2006,** *359*, 224-229.
48. Chang, J.-L.; Wei, G.-T.; Zen, J.-M., Screen-Printed Ionic Liquid/Preanodized Carbon Electrode: Effective Detection of Dopamine in the Presence of High Concentration of Ascorbic Acid. *Electrochem. Commun.* **2011,** *13*, 174-177.
49. Wu, L.; Feng, L.; Ren, J.; Qu, X., Electrochemical Detection of Dopamine using Porphyrin-Functionalized Graphene. *Biosens. Bioelectron* **2012,** *34*, 57-62.
50. Kim, Y.-R.; Bong, S.; Kang, Y.-J.; Yang, Y.; Mahajan, R. K.; Kim, J. S.; Kim, H., Electrochemical Detection of Dopamine in the Presence of Ascorbic Acid using Graphene Modified Electrodes. *Biosens. Bioelectron* **2010,** *25*, 2366-2369.
51. Liu, S.; Yan, J.; He, G.; Zhong, D.; Chen, J.; Shi, L.; Zhou, X.; Jiang, H., Layer-by-Layer Assembled Multilayer Films of Reduced Graphene Oxide/Gold Nanoparticles for the Electrochemical Detection of Dopamine. *J. Electroanal. Chem.* **2012,** *672*, 40-44.
52. Wang, Y.; Li, Y. M.; Tang, L. H.; Lu, J.; Li, J. H., Application of Graphene-Modified Electrode for Selective Detection of Dopamine. *Electrochem. Commun.* **2009,** *11*, 889-892.
53. Sun, C.-L.; Lee, H.-H.; Yang, J.-M.; Wu, C.-C., The Simultaneous Electrochemical Detection of Ascorbic Acid, Dopamine, and Uric Acid using Graphene/Size-Selected Pt Nanocomposites. *Biosens. Bioelectron.* **2011,** *26*, 3450-3455.
54. Zhang, M.; Gong, K.; Zhang, H.; Mao, L., Layer-by-Layer Assembled Carbon Nanotubes for Selective Determination of Dopamine in the Presence of Ascorbic Acid. *Biosens. Bioelectron.* **2005,** *20*, 1270-1276.
55. Jiang, L.; Nelson, G. W.; Abda, J.; Foord, J. S., Novel Modifications to Carbon-Based Electrodes to Improve the Electrochemical Detection of Dopamine. *ACS Appl. Mater. Interfaces* **2016,** *8*, 28338-28348.
56. Tan, C.; Cao, X.; Wu, X.-J.; He, Q.; Yang, J.; Zhang, X.; Chen, J.; Zhao, W.; Han, S.; Nam, G.-H.; Sindoro, M.; Zhang, H., Recent Advances in Ultrathin Two-Dimensional Nanomaterials. *Chem. Rev.* **2017,** *117*, 6225-6331.
57. Abdulbari, H. A.; Basheer, E. A. M., Electrochemical Biosensors: Electrode Development, Materials, Design, and Fabrication. *ChemBioEng Rev.* **2017,** *4*, 92-105.

58. Hmadeh, M.; Lu, Z.; Liu, Z.; Gándara, F.; Furukawa, H.; Wan, S.; Augustyn, V.; Chang, R.; Liao, L.; Zhou, F.; Perre, E.; Ozolins, V.; Suenaga, K.; Duan, X.; Dunn, B.; Yamamto, Y.; Terasaki, O.; Yaghi, O. M., New Porous Crystals of Extended Metal-Catecholates. *Chem. Mater.* **2012,** *24*, 3511-3513.
59. Ko, M.; Mendecki, L.; Mirica, K. A., Conductive Two-Dimensional Metal–Organic Frameworks as Multifunctional Materials. *Chem. Commun.* **2018,** *54*, 7873-7891.
60. Campbell, M. G.; Sheberla, D.; Liu, S. F.; Swager, T. M.; Dincă, M., Cu_3(hexaiminotriphenylene)$_2$: An Electrically Conductive 2D Metal-Organic Framework for Chemiresistive Sensing. *Angew. Chem., Int. Ed.* **2015,** *54*, 4349-4352.
61. Campbell, M. G.; Liu, S. F.; Swager, T. M.; Dincă, M., Chemiresistive Sensor Arrays from Conductive 2D Metal–Organic Frameworks. *J. Am. Chem. Soc.* **2015,** *137*, 13780-13783.
62. Smith, M. K.; Jensen, K. E.; Pivak, P. A.; Mirica, K. A., Direct Self-Assembly of Conductive Nanorods of Metal–Organic Frameworks into Chemiresistive Devices on Shrinkable Polymer Films. *Chem. Mater.* **2016,** *28*, 5264-5268.
63. Ko, M.; Aykanat, A.; Smith, M.; Mirica, K., Drawing Sensors with Ball-Milled Blends of Metal-Organic Frameworks and Graphite. *Sensors* **2017,** *17*, 2192.
64. Yao, M.-S.; Lv, X.-J.; Fu, Z.-H.; Li, W.-H.; Deng, W.-H.; Wu, G.-D.; Xu, G., Layer-by-Layer Assembled Conductive Metal-Organic Framework Nanofilms for Room-Temperature Chemiresistive Sensing. *Angew. Chem.* **2017**.
65. Smith, M. K.; Mirica, K. A., Self-Organized Frameworks on Textiles (SOFT): Conductive Fabrics for Simultaneous Sensing, Capture, and Filtration of Gases. *J. Am. Chem. Soc.* **2017,** *139*, 16759-16767.
66. Mendecki, L.; Mirica, K. A., Conductive Metal–Organic Frameworks as Ion-to-Electron Transducers in Potentiometric Sensors. *ACS Appl. Mater. Interfaces* **2018,** *10*, 19248-19257.
67. Li, W. H.; Ding, K.; Tian, H. R.; Yao, M. S.; Nath, B.; Deng, W. H.; Wang, Y. B.; Xu, G., Conductive Metal-Organic Framework Nanowire Array Electrodes for High-Performance Solid-State Supercapacitors. *Adv. Funct. Mater.* **2017,** *27*, 1702067.
68. Sheberla, D.; Bachman, J. C.; Elias, J. S.; Sun, C. J.; Shao-Horn, Y.; Dincă, M., Conductive MOF Electrodes for Stable Supercapacitors with High Areal Capacitance. *Nat. Mater.* **2017,** *16*, 220-224.
69. Feng, D.; Lei, T.; Lukatskaya, M. R.; Park, J.; Huang, Z.; Lee, M.; Shaw, L.; Chen, S.; Yakovenko, A. A.; Kulkarni, A.; Xiao, J.; Fredrickson, K.; Tok, J. B.; Zou, X.; Cui, Y.; Bao, Z., Robust and conductive Two-Dimensional Metal–Organic Frameworks with Exceptionally High Volumetric and Areal Capacitance. *Nat. Energy* **2018,** *3*, 30-36.
70. Downes, C. A.; Clough, A. J.; Chen, K.; Yoo, J. W.; Marinescu, S. C., Evaluation of the H_2 Evolving Activity of Benzenehexathiolate Coordination Frameworks and the Effect of Film Thickness on H_2 Production. *ACS Appl. Mater. Interfaces* **2018,** *10*, 1719-1727.
71. Clough, A. J.; Yoo, J. W.; Mecklenburg, M. H.; Marinescu, S. C., Two-Dimensional Metal–Organic Surfaces for Efficient Hydrogen Evolution from Water. *J. Am. Chem. Soc.* **2015,** *137*, 118-121.
72. Dong, R.; Pfeffermann, M.; Liang, H.; Zheng, Z.; Zhu, X.; Zhang, J.; Feng, X., Large-Area, Free-Standing, Two-Dimensional Supramolecular Polymer Single-Layer Sheets for Highly Efficient Electrocatalytic Hydrogen Evolution. *Angew. Chem., Int. Ed.* **2015,** *54*, 12058-12063.
73. Miner, E. M.; Fukushima, T.; Sheberla, D.; Sun, L.; Surendranath, Y.; Dincă, M., Electrochemical Oxygen Reduction Catalysed by Ni_3(hexaiminotriphenylene)$_2$. *Nat. Commun.* **2016,** *7*, 10942.
74. Huang, X.; Yao, H.; Cui, Y.; Hao, W.; Zhu, J.; Xu, W.; Zhu, D., Conductive Copper Benzenehexathiol Coordination Polymer as a Hydrogen Evolution Catalyst. *ACS Appl. Mater. Interfaces* **2017,** *9*, 40752-40759.
75. Sun, X.; Wu, K.-H.; Sakamoto, R.; Kusamoto, T.; Maeda, H.; Ni, X.; Jiang, W.; Liu, F.; Sasaki, S.; Masunaga, H.; Nishihara, H., Bis(aminothiolato)Nickel Nanosheet as a Redox switch for Conductivity and an Electrocatalyst for the Hydrogen Evolution Reaction. *Chem. Sci.* **2017,** *8*, 8078-8085.
76. Jia, H.; Yao, Y.; Zhao, J.; Gao, Y.; Luo, Z.; Du, P., A Novel Two-Dimensional Nickel Phthalocyanine-Based Metal–Organic Framework for Highly Efficient Water Oxidation Catalysis. *J. Mater. Chem. A* **2018,** *6*, 1188-1195.
77. Mendecki, L.; Ko, M.; Zhang, X.; Meng, Z.; Mirica, K. A., Porous Scaffolds for Electrochemically Controlled Reversible Capture and Release of Ethylene. *J. Am. Chem. Soc.* **2017,** *139*, 17229-17232.
78. Wu, F.; Fang, W.; Yang, X.; Xu, J.; Xia, J.; Wang, Z., Two-Dimensional π-Conjugated Metal-Organic Framework with High Electrical Conductivity for Electrochemical Sensing. *J. Chin. Chem. Soc.* **2018,** *66*, 522-528.
79. Tan, H.; Ma, C.; Gao, L.; Li, Q.; Song, Y.; Xu, F.; Wang, T.; Wang, L., Metal-Organic Framework-Derived Copper Nanoparticle@Carbon Nanocomposites as Peroxidase Mimics for Colorimetric Sensing of Ascorbic Acid. *Chem. Eur. J.* **2014,** *20*, 16377-16383.
80. Zhang, J. W.; Zhang, H. T.; Du, Z. Y.; Wang, X.; Yu, S. H.; Jiang, H. L., Water-Stable Metal-Organic Frameworks with Intrinsic Peroxidase-Like Catalytic Activity as a Colorimetric Biosensing Platform. *Chem. Commun.* **2014,** *50*, 1092-1094.
81. Yue, D.; Zhao, D.; Zhang, J.; Zhang, L.; Jiang, K.; Zhang, X.; Cui, Y.; Yang, Y.; Chen, B.; Qian, G., A Luminescent Cerium Metal-Organic Framework for the Turn-on Sensing of Ascorbic Acid. *Chem. Commun.* **2017,** *53*, 11221-11224.
82. Yue, D.; Huang, Y.; Zhang, J.; Zhang, X.; Cui, Y.; Yang, Y.; Qian, G., A Two-Dimensional Metal-Organic Framework as a Fluorescent Probe for Ascorbic Acid Sensing. *Eur. J. Inorg. Chem.* **2018,** *2018*, 173-177.
83. Wu, S.; Lin, Y.; Liu, J.; Shi, W.; Yang, G.; Cheng, P., Rapid Detection of the Biomarkers for Carcinoid Tumors by a Water Stable Luminescent Lanthanide Metal-Organic Framework Sensor. *Adv. Func. Mater.* **2018,** *28*, 1707169.
84. Shen, W.-J.; Zhuo, Y.; Chai, Y.-Q.; Yuan, R., Ce-based metal-Organic Frameworks and DNAzyme-Assisted Recycling as Dual Signal Amplifiers for Sensitive Electrochemical Detection of Lipopolysaccharide. *Biosens. Bioelectron.* **2016,** *83*, 287-292.
85. Wei, Z.; Zhu, W.; Li, Y.; Ma, Y.; Wang, J.; Hu, N.; Suo, Y.; Wang, J., Conductive Leaflike Cobalt Metal–Organic Framework Nanoarray on Carbon Cloth as a Flexible and

Versatile Anode toward Both Electrocatalytic Glucose and Water Oxidation. *Inorg. Chem.* **2018,** *57*, 8422-8428.
86. Zhang, W.; Jia, G.; Li, Z.; Yuan, C.; Bai, Y.; Fu, D., Selective Electrochemical Detection of Dopamine on Polyoxometalate-Based Metal-Organic Framework and Its Composite with Reduced Graphene Oxide. *Adv. Mater. Interfaces* **2017,** *4*, 1601241.
87. Ma, W.; Jiang, Q.; Yu, P.; Yang, L.; Mao, L., Zeolitic Imidazolate Framework-Based Electrochemical Biosensor for in Vivo Electrochemical Measurements. *Anal. Chem.* **2013,** *85*, 7550-7557.
88. Liu, W.; Yin, X.-B., Metal–Organic Frameworks for Electrochemical Applications. *TrAC Trends Anal. Chem.* **2016,** *75*, 86-96.
89. Campbell, M.; Dincă, M., Metal–Organic Frameworks as Active Materials in Electronic Sensor Devices. *Sensors* **2017,** *17*, 1108.
90. Hosseini, H.; Ahmar, H.; Dehghani, A.; Bagheri, A.; Tadjarodi, A.; Fakhari, A. R., A Novel Electrochemical Sensor Based on Metal-Organic Framework for Electro-Catalytic Oxidation of L-Cysteine. *Biosens. Bioelectron.* **2013,** *42*, 426-429.
91. Li, Y.; Huangfu, C.; Du, H.; Liu, W.; Li, Y.; Ye, J., Electrochemical Behavior of Metal–Organic Framework MIL-101 Modified Carbon Paste Electrode: An Excellent Candidate for Electroanalysis. *J. Electroanal. Chem.* **2013,** *709*, 65-69.
92. Liu, S.; Xing, X.; Yu, J.; Lian, W.; Li, J.; Cui, M.; Huang, J., A Novel Label-Free Electrochemical Aptasensor based on Graphene–Polyaniline Composite Film for Dopamine Determination. *Biosens. Bioelectron.* **2012,** *36*, 186-191.
93. Nakatsuka, N.; Yang, K. A.; Abendroth, J. M.; Cheung, K. M.; Xu, X.; Yang, H.; Zhao, C.; Zhu, B.; Rim, Y. S.; Yang, Y.; Weiss, P. S.; Stojanovic, M. N.; Andrews, A. M., Aptamer-Field-Effect Transistors Overcome Debye Length Limitations for Small-Molecule Sensing. *Science* **2018,** *362*, 319-324.
94. Chavez, J. L.; Hagen, J. A.; Kelley-Loughnane, N., Fast and Selective Plasmonic Serotonin Detection with Aptamer-Gold Nanoparticle Conjugates. *Sensors* **2017,** *17*.
95. Liu, Q.; Zhu, X.; Huo, Z.; He, X.; Liang, Y.; Xu, M., Electrochemical Detection of dopamine in the Presence of Ascorbic Acid using PVP/Graphene Modified Electrodes. *Talanta* **2012,** *97*, 557-562.
96. Yola, M. L.; Atar, N., A Novel Detection Approach for Serotonin by Graphene Quantum Dots/Two-Dimensional (2D) Hexagonal Boron Nitride Nanosheets with Molecularly Imprinted Polymer. *Appl. Surf. Sci.* **2018,** *458*, 648-655.
97. Tan, L.; Zhou, K.-G.; Zhang, Y.-H.; Wang, H.-X.; Wang, X.-D.; Guo, Y.-F.; Zhang, H.-L., Nanomolar Detection of Dopamine in the Presence of Ascorbic Acid at β-Cyclodextrin/Graphene Nanocomposite Platform. *Electrochem. Commun.* **2010,** *12*, 557-560.
98. Yaghi, O. M.; O'Keeffe, M.; Ockwig, N. W.; Chae, H. K.; Eddaoudi, M.; Kim, J., Reticular Synthesis and the Design of New Materials. *Nature* **2003,** *423*, 705-714.
99. Sheberla, D.; Sun, L.; Blood-Forsythe, M. A.; Er, S.; Wade, C. R.; Brozek, C. K.; Aspuru-Guzik, A.; Dincă, M., High Electrical Conductivity in Ni3 (2,3,6,7,10,11-hexaiminotriphenylene)2, a Semiconducting Metal–Organic Graphene Analogue. *J. Am. Chem. Soc.* **2014,** *136*, 8859-8862.
100. Zheng, Z.; Qiu, H.; Zheng, M.; Weng, S.; Huang, Z.; Xian, R.; Lin, X., Selective Electrochemical Determination of Dopamine in Serum in the Presence of Ascorbic Acid and Uric Acid by using a CuO Nanoleaf Electrode. *Anal. Methods* **2014,** *6*, 7923-7927.
101. Khudaish, E. A.; Farsi, A. A. A., Electrochemical Oxidation of Dopamine and Ascorbic Acid at a Palladium Electrode Modified with in situ Fabricated Iodine-Adlayer in Alkaline Solution. *Talanta* **2010,** *80*, 1919-1925.
102. Mitchell, E. C.; Dunaway, L. E.; McCarty, G. S.; Sombers, L. A., Spectroelectrochemical Characterization of the Dynamic Carbon-Fiber Surface in Response to Electrochemical Conditioning. *Langmuir* **2017,** *33*, 7838-7846.
103. Cao, Q.; Puthongkham, P.; Venton, B. J., Review: New Insights into Optimizing Chemical and 3D Surface Structures of Carbon Electrodes for Neurotransmitter Detection. *Anal. Methods* **2019,** *11*, 247-261.
104. Wang, Y.; Li, Y.; Tang, L.; Lu, J.; Li, J., Application of graphene-modified electrode for selective detection of dopamine. *Electrochem. Commun.* **2009,** *11*, 889-892.
105. Jacobs, C. B.; Vickrey, T. L.; Venton, B. J., Functional Groups Modulate the Sensitivity and Electron Transfer Kinetics of Neurochemicals at Carbon Nanotube Modified Microelectrodes. *Analyst* **2011,** *136*, 3557-3565.
106. Liu, B.; Ouyang, X.; Ding, Y.; Luo, L.; Xu, D.; Ning, Y., Electrochemical Preparation of Nickel and Copper Oxides-Decorated Graphene Composite for Simultaneous Determination of Dopamine, Acetaminophen and Tryptophan. *Talanta* **2016,** *146*, 114-121.
107. Ulubay, S.; Dursun, Z., Cu nanoparticles Incorporated Polypyrrole Modified GCE for Sensitive Simultaneous Determination of Dopamine and Uric Acid. *Talanta* **2010,** *80*, 1461-1466.
108. Pihel, K.; Walker, Q. D.; Wightman, R. M., Overoxidized Polypyrrole-Coated Carbon Fiber Microelectrodes for Dopamine Measurements with Fast-Scan Cyclic Voltammetry. *Anal. Chem.* **1996,** *68*, 2084-2089.
109. Gileadi, E., *Electrode Kinetics for Chemists, Chemical Engineers and Materials Scientists*. Capstone: 1993;
110. Wang, J., Electrochemical Detection for Microscale Analytical Systems: A Review. *Talanta* **2002,** *56*, 223-231.
111. Weber, S. G.; Purdy, W. C., Electrochemical Detectors in Liquid Chromatography. A Short Review of Detector Design. *Ind. Eng. Chem. Prod. Res. Dev.* **1981,** *20*, 593-598.
112. Wijeratne, K.; Ail, U.; Brooke, R.; Vagin, M.; Liu, X.; Fahlman, M.; Crispin, X., Bulk Electronic Transport Impacts on Electron Transfer at Conducting Polymer Electrode-Electrolyte Interfaces. *Proc. Natl. Acad. Sci. U. S. A.* **2018,** *115*, 11899-11904.
113. Ambolikar, A. S.; Guin, S. K.; Neogy, S., An Insight into the Outer- and Inner-sphere Electrochemistry of Oxygenated Single-Walled Carbon Nanohorns (o-SWCNHs). *New J. Chem.* **2019**.
114. Schauff, S.; Ciorca, M.; Laforgue, A.; Bélanger, D., Electron Transfer Processes at Aryl-Modified Glassy Carbon Electrode. *Electroanalysis* **2009,** *21*, 1499-1504.
115. Chen, Q.; Espey, M. G.; Krishna, M. C.; Mitchell, J. B.; Corpe, C. P.; Buettner, G. R.; Shacter, E.; Levine, M., Pharmacologic Ascorbic Acid Concentrations Selectively Kill Cancer Cells: Action as a Pro-Drug to Deliver Hydrogen

Peroxide to Tissues. *Proc. Natl. Acad. Sci. U.S.A.* **2005,** *102*, 13604-13609.
116. Bryson, G.; Bischoff, F., Dopamine Transport in Blood. *Clin. Chem* **1970,** *16*, 312-317.
117. Enomoto, A.; Kimura, H.; Chairoungdua, A.; Shigeta, Y.; Jutabha, P.; Cha, S. H.; Hosoyamada, M.; Takeda, M.; Sekine, T.; Igarashi, T.; Matsuo, H.; Kikuchi, Y.; Oda, T.; Ichida, K.; Hosoya, T.; Shimokata, K.; Niwa, T.; Kanai, Y.; Endou, H., Molecular Identification of a Renal Urate Anion Exchanger that Regulates Blood Urate Levels. *Nature* **2002,** *417*, 447-452.
118. Sharma, S.; Singh, N.; Tomar, V.; Chandra, R., A Review on Electrochemical Detection of Serotonin Based on Surface Modified Electrodes. *Biosens. Bioelectron.* **2018,** *107*, 76-93.
119. Hu, I. F.; Kuwana, T., Oxidative Mechanism of Ascorbic Acid at Glassy Carbon Electrodes. *Anal. Chem.* **1986,** *58*, 3235-3239.
120. Warren, J. J.; Mayer, J. M., Tuning of the Thermochemical and Kinetic Properties of Ascorbate by Its Local Environment: Solution Chemistry and Biochemical Implications. *J. Am. Chem. Soc.* **2010,** *132*, 7784-7793.
121. Pisoschi, A. M.; Pop, A.; Serban, A. I.; Fafaneata, C., Electrochemical Methods for Ascorbic Acid Determination. *Electrochimica Acta.* **2014,** *121*, 443-460.
122. Klunder, K. J.; Nilsson, Z.; Sambur, J. B.; Henry, C. S., Patternable Solvent-Processed Thermoplastic Graphite Electrodes. *J. Am. Chem. Soc.* **2017,** *139*, 12623-12631.
123. Peltola, E.; Sainio, S.; Holt, K. B.; Palomäki, T.; Koskinen, J.; Laurila, T., Electrochemical Fouling of Dopamine and Recovery of Carbon Electrodes. *Anal. Chem.* **2018,** *90*, 1408-1416.
124. Nantaphol, S.; Channon, R. B.; Kondo, T.; Siangproh, W.; Chailapakul, O.; Henry, C. S., Boron Doped Diamond Paste Electrodes for Microfluidic Paper-Based Analytical Devices. *Anal. Chem.* **2017,** *89*, 4100-4107.
125. Day, R. W.; Bediako, D. K.; Rezaee, M.; Parent, L. R.; Skorupskii, G.; Arguilla, M. Q.; Hendon, C. H.; Stassen, I.; Gianneschi, N. C.; Kim, P.; Dincă, M., Single Crystals of Electrically Conductive Two-Dimensional Metal-Organic Frameworks: Structural and Electrical Transport Properties. *ACS Cent. Sci.* **2019,** *5*, 1959-1964.
126. Mikolajczyk, A.; Gajewicz, A.; Rasulev, B.; Schaeublin, N.; Maurer-Gardner, E.; Hussain, S.; Leszczynski, J.; Puzyn, T., Zeta Potential for Metal Oxide Nanoparticles: A Predictive Model Developed by a Nano-Quantitative Structure–Property Relationship Approach. *Chem. Mater.* **2015,** *27*, 2400-2407.
127. Gibson, N.; Shenderova, O.; Luo, T. J. M.; Moseenkov, S.; Bondar, V.; Puzyr, A.; Purtov, K.; Fitzgerald, Z.; Brenner, D. W., Colloidal Stability of Modified Nanodiamond Particles. *Diam. Relat. Mater.* **2009,** *18*, 620-626.
128. Hopkins, E.; Sharma, S., *Physiology, Acd Base Balance*. StatPearls Publishing: Treasure Island, 2019;
129. Abazari, R.; Mahjoub, A. R.; Ataei, F.; Morsali, A.; Carpenter-Warren, C. L.; Mehdizadeh, K.; Slawin, A. M. Z., Chitosan Immobilization on Bio-MOF Nanostructures: A Biocompatible pH-Responsive Nanocarrier for Doxorubicin Release on MCF-7 Cell Lines of Human Breast Cancer. *Inorg. Chem.* **2018,** *57*, 13364-13379.
130. S, M.; Raj, K.; Reddy, A. P., Cyclic Voltammetric Studies of the Interaction of Rizatriptan Benzoate with Copper in Aqueous Solution. *Int. Res. J. Pharm.* **2017,** *8*, 117-121.
131. Naidek, K. P.; Zuconelli, C. R.; Cruz, O. M.; Ribeiro, R.; Winnischofer, S. M. B.; Winnischofer, H., Characterization of 2,3,6,7,10,11-hexahydroxytriphenylene and its effects on cell viability in human cancer cell lines. *Biochem. Cell Biol.* **2016,** *94*, 205-211.
132. Loera-Serna, S.; Oliver-Tolentino, M. A.; de Lourdes López-Núñez, M.; Santana-Cruz, A.; Guzmán-Vargas, A.; Cabrera-Sierra, R.; Beltrán, H. I.; Flores, J., Electrochemical behavior of $[Cu_3(BTC)_2]$ metal–organic framework: The effect of the method of synthesis. *J. Alloys Compd.* **2012,** *540*, 113-120.
133. Barthram, A. M.; Cleary, R. L.; Kowallick, R.; Ward, M. D., A New Redox-Tunable Near-IR Dye Based on a Trinuclear Ruthenium(II) Complex of Hexahydroxytriphenylene. *Chem. Comun.* **1998,** 2695-2696.
134. Grange, C. S.; Meijer, A. J.; Ward, M. D., Trinuclear Ruthenium Dioxolene Complexes based on the Bridging Ligand Hexahydroxytriphenylene: Electrochemistry, Spectroscopy, and Near-Infrared Electrochromic Behaviour Associated with a Reversible Seven-Membered Redox Chain. *Dalton Trans.* **2010,** *39*, 200-211.
135. Punckt, C.; Pope, M. A.; Aksay, I. A., On the Electrochemical Response of Porous Functionalized Graphene Electrodes. *J. Phys. Chem. C* **2013,** *117*, 16076-16086.
136. Muhammad, H.; Tahiri, I. A.; Muhammad, M.; Masood, Z.; Versiani, M. A.; Khaliq, O.; Latif, M.; Hanif, M., A Comprehensive heterogeneous Electron Transfer Rate Constant Evaluation of Dissolved Oxygen in DMSO at Glassy Carbon Electrode Measured by Different Electrochemical Methods. *J. Electroanal. Chem.* **2016,** *775*, 157-162.
137. Peng, Z.; Yi, X.; Liu, Z.; Shang, J.; Wang, D., Triphenylamine-Based Metal–Organic Frameworks as Cathode Materials in Lithium-Ion Batteries with Coexistence of Redox Active Sites, High Working Voltage, and High Rate Stability. *ACS Appl. Mater. Interfaces* **2016,** *8*, 14578-14585.
138. Wong, C. H. A.; Pumera, M., Surfactants Show both Large Positive and Negative Effects on Observed Electron Transfer Rates at Thermally Reduced Graphenes. *Electrochem.* **2012,** *22*, 105-108.
139. Foster, C. W.; Brownson, D. A.; Ruas de Souza, A. P.; Bernalte, E.; Iniesta, J.; Bertotti, M.; Banks, C. E., Pencil it in: Pencil Drawn Electrochemical Sensing Platforms. *Analyst* **2016,** *141*, 4055-4064.
140. Ji, X.; Banks, C. E.; Crossley, A.; Compton, R. G., Oxygenated Edge Plane Sites Slow the Electron Transfer of the Ferro-/Ferricyanide Redox Couple at Graphite Electrodes. *Chemphyschem* **2006,** *7*, 1337-1344.
141. Randviir, E. P.; Brownson, D. A.; Metters, J. P.; Kadara, R. O.; Banks, C. E., The Fabrication, Characterisation and Electrochemical Investigation of Screen-Printed Graphene Electrodes. *Phys. Chem. Chem. Phys.* **2014,** *16*, 4598-4611.
142. Pumera, M.; Sasaki, T.; Iwai, H., Relationship between Carbon Nanotube Structure and Electrochemical Behavior: Heterogeneous Electron Transfer at

Electrochemically Activated Carbon Nanotubes. *Chem. Asian J.* **2008,** *3*, 2046-2055.
143. Kempton, J. H.; Lindberg, R. D.; Runnells, D. D., Numerical modeling of platinum Eh measurements by using heterogeneous electron-transfer kinetics. ACS Publications: 1990.
144. Abou-Elela, A., Epidemiology, Pathophysiology, and Management of Uric Acid Urolithiasis: A Narrative Review. *J. Adv. Res.* **2017,** *8*, 513-527.
145. Berfield, J. L.; Wang, L. C.; Reith, M. E., Which Form of Dopamine is the Substrate For the Human Dopamine Transporter: The Cationic or the Uncharged Species? *J. Biol. Chem.* **1999,** *274*, 4876-4882.
146. Pratuangdejkul, J.; Nosoongnoen, W.; Guérin, G.-A.; Loric, S.; Conti, M.; Launay, J.-M.; Manivet, P., Conformational Dependence of Serotonin Theoretical pKa Prediction. *Chem. Phys. Lett.* **2006,** *420*, 538-544.
147. Albrecht, T., Kulandainatha, M. A., Amemiya, S., Boukherroub, R., Burrows, A. D, Carminati, M., Dale, S. E.C., Ferrari, G., Halls, J., E., Huang, X.J., Jiang, D., Jiang, Y., X., Kant, R., Kaur, J., Li, J. T., Marken, F., Mirkin, M. V., Nuttall, P., Pitchford, W., Ren, B., Rutkowska, A. J., Schmuki, P., Shrestha, N. K., Singh, M. B., Sun, C. F., Szunerits, S., Wain, A. J., Wang, Y., Yu, X. Y. *Electrochemistry*. Royal Society of Chemistry: Cambridge, 2013; Vol. 12.
148. Brownson, D. A. C.; Munro, L. J.; Kampouris, D. K.; Banks, C. E., Electrochemistry of Graphene: Not Such a Beneficial Electrode Material? *RSC Adv.* **2011,** *1*, 978-988.
149. Rocha, L. S.; Carapuça, H. M., Ion-Exchange Voltammetry of dopamine at Nafion-Coated Glassy Carbon Electrodes: Quantitative Features of Ion-Exchange Partition and Reassessment on the Oxidation Mechanism of Dopamine in the Presence of Excess Ascorbic Acid. *Bioelectrochemistry* **2006,** *69*, 258-266.
150. Marsh, H. A.; Dryhurst, G., Enzymatic and Electrochemical Oxidation of Uric Acid. *J. Electroanl. chem. Interfacial Electrochem.* **1979,** *95*, 81-90.
151. Struck, W. A.; Elving, P. J., Electrolytic Oxidation of Uric Acid: Products and Mechanism*. *Biochemistry* **1965,** *4*, 1343-1353.
152. Owens, J. L.; Marsh, H. A.; Dryhurst, G., Electrochemical Oxidation of Uric Acid and Xanthine. *J. Electroanl. Chem. Interfacial Electrochem.* **1978,** *91*, 231-247.
153. Goyal, R. N.; Gupta, V. K.; Sangal, A.; Bachheti, N., Voltammetric Determination of Uric Acid at a Fullerene-C60-Modified Glassy Carbon Electrode. *Electroanalysis* **2005,** *17*, 2217-2223.
154. Jin, G.-P.; Lin, X.-Q.; Ding, Y.-F., Glassy Carbon Electrodes Modified with Mixed Covalent Monolayers of Choline, Glycine, and Glutamic Acid for the Determination of Phenolic Compounds. *J. Solid State Electrochem.* **2006,** *10*, 987-994.
155. Sajid, M.; Nazal, M. K.; Mansha, M.; Alsharaa, A.; Jillani, S. M. S.; Basheer, C., Chemically Modified Electrodes for Electrochemical Detection of Dopamine in the Presence of Uric Acid and Ascorbic Acid: A Review. *TrAC Trends in Anal. Chem.* **2016,** *76*, 15-29.
156. Bard, A. J.; Faulkner, L. R., *Electrochemical Methods: Fundamentals and Applications*. 2nd ed ed.; Wiley: New York, 2001; Vol 2
157. Shang, N. G.; Papakonstantinou, P.; McMullan, M.; Chu, M.; Stamboulis, A.; Potenza, A.; Dhesi, S. S.; Marchetto, H., Catalyst-Free Efficient Growth, Orientation and Biosensing Properties of Multilayer Graphene Nanoflake Films with Sharp Edge Planes. *Adv. Func. Mater.* **2008,** *18*, 3506-3514.
158. Zachek, M. K.; Hermans, A.; Wightman, R. M.; McCarty, G. S., Electrochemical Dopamine Detection: Comparing Gold and Carbon Fiber Microelectrodes using Background Subtracted Fast Scan Cyclic Voltammetry. *J. Electroanal. Chem.* **2008,** *614*, 113-120.
159. Gao, F.; Cai, X.; Wang, X.; Gao, C.; Liu, S.; Gao, F.; Wang, Q., Highly Sensitive and Selective Detection of Dopamine in the Presence of Ascorbic Acid at Graphene Oxide Modified Electrode. *Sens. and Actu B. Chem.* **2013,** *186*, 380-387.
160. Khan, A. F.; Brownson, D. A. C.; Randviir, E. P.; Smith, G. C.; Banks, C. E., 2D Hexagonal Boron Nitride (2D-hBN) Explored for the Electrochemical Sensing of Dopamine. *Anal. Chem.* **2016,** *88*, 9729-9737.
161. Cruz Moraes, F.; Cabral, M. F.; Machado, S. A. S.; Mascaro, L. H., Electrocatalytic Behavior of Glassy Carbon Electrodes Modified with Multiwalled Carbon Nanotubes and Cobalt Phthalocyanine for Selective Analysis of Dopamine in Presence of Ascorbic Acid. *Electroanalysis* **2008,** *20*, 851-857.
162. Cournil, I.; Geffard, M.; Moulins, M.; Le Moal, M., Coexistence of Dopamine and Serotonin in an Identified Neuron of the Lobster Nervous System. *Brain Res.* **1984,** *310*, 397-400.
163. Ghita, M.; Arrigan, D. W. M., Dopamine Voltammetry at Overoxidised Polyindole Electrodes. *Electrochimica Acta.* **2004,** *49*, 4743-4751.
164. Chia, X.; Eng, A. Y.; Ambrosi, A.; Tan, S. M.; Pumera, M., Electrochemistry of Nanostructured Layered Transition-Metal Dichalcogenides. *Chem Rev* **2015,** *115*, 11941-11966.
165. Nikolelis, D. P.; Drivelos, D. A.; Simantiraki, M. G.; Koinis, S., An Optical Spot Test for the Detection of Dopamine in Human Urine using Stabilized in Air Lipid Films. *Anal. Chem.* **2004,** *76*, 2174-2180.
166. Nichkova, M. I.; Huisman, H.; Wynveen, P. M.; Marc, D. T.; Olson, K. L.; Kellermann, G. H., Evaluation of a Novel ELISA for Serotonin: Urinary Serotonin as a Potential Biomarker for Depression. *Anal. Bioanal. Chem.* **2012,** *402*, 1593-1600.
167. Feldman, J. M., Urinary Serotonin in the Diagnosis of Carcinoid Tumors. *Clin. Chem.* **1986,** *32*, 41-48.
168. Nichkova, M.; Wynveen, P. M.; Marc, D. T.; Huisman, H.; Kellermann, G. H., Validation of an ELISA for Urinary Dopamine: Applications in Monitoring Treatment of Dopamine-Related Disorders. *J. Neurochem.* **2013,** *125*, 724-735.
169. Brooks, T.; Keevil, C. W., A Simple Artificial Urine for the Growth of Urinary Pathogens. *Lett. Appl. Microbiol.* **1997,** *24*, 203-206.
170. Satyanarayana, M.; Reddy, K. K.; Gobi, K. V., Nanobiocomposite Based Electrochemical Sensor for Sensitive Determination of Serotonin in Presence of Dopamine, Ascorbic Acid and Uric Acid In Vitro. *Electroanalysis* **2014,** *26*, 2365-2372.

171. Ellerbee, A. K.; Phillips, S. T.; Siegel, A. C.; Mirica, K. A.; Martinez, A. W.; Striehl, P.; Jain, N.; Prentiss, M.; Whitesides, G. M., Quantifying Colorimetric Assays in Paper-Based Microfluidic Devices by Measuring the Transmission of Light Through Paper. *Anal. Chem.* **2009,** *81*, 8447-8452.
172. Tang, H. Y.; Beer, L. A.; Speicher, D. W., In-Depth Analysis of a Plasma or Serum Proteome Using a 4D Protein Profiling Method. *Methods Mol. Biol.* **2011,** *728*, 47-67.
173. D'Silva, A. M.; Hyett, J. A.; Coorssen, J. R., A Routine 'Top-Down' Approach to Analysis of the Human Serum Proteome. *Proteomes* **2017,** *5*, 13.
174. Ge, P.-Y.; Du, Y.; Xu, J.-J.; Chen, H.-Y., Selective Detection of Dopamine Based on the Unique Property of Gold Nanofilm. *J. Electroanal. Chem.* **2009,** *633*, 182-186.
175. Zhou, C.; Li, S.; Zhu, W.; Pang, H.; Ma, H., A Sensor of a Polyoxometalate and Au–Pd Alloy for Simultaneously Detection of Dopamine and Ascorbic Acid. *Electrochim. Acta* **2013,** *113*, 454-463.
176. Kachoosangi, R. T.; Compton, R. G., A Simple Electroanalytical Methodology for the Simultaneous Determination of Dopamine, Serotonin And Ascorbic Acid using an Unmodified Edge Plane Pyrolytic Graphite Electrode. *Anal. Bioanal. Chem.* **2007,** *387*, 2793-2800.
177. Sun, W.; Wang, X.; Wang, Y.; Ju, X.; Xu, L.; Li, G.; Sun, Z., Application of Graphene–SnO2 Nanocomposite Modified Electrode for the Sensitive Electrochemical Detection of Dopamine. *Electrochim. Acta* **2013,** *87*, 317-322.
178. Cesarino, I.; Galesco, H. V.; Machado, S. A., Determination of Serotonin on Platinum Electrode Modified with Carbon Nanotubes/Polypyrrole/Silver Nanoparticles Nanohybrid. *Mater. Sci. Eng. C Mater. Biol. Appl.* **2014,** *40*, 49-54.
179. Xue, C.; Wang, X.; Zhu, W.; Han, Q.; Zhu, C.; Hong, J.; Zhou, X.; Jiang, H., Electrochemical Serotonin Sensing Interface Based on Double-Layered Membrane of Reduced Graphene Oxide/Polyaniline Nanocomposites and Molecularly Imprinted Polymers Embedded with Gold Nanoparticles. *Sens. and Actu B. Chem.* **2014,** *196*, 57-63.
180. Anithaa, A. C.; Asokan, K.; Sekar, C., Highly Sensitive and Selective Serotonin Sensor Based on Gamma Ray Irradiated Tungsten Trioxide Nanoparticles. *Sens. and Actu B. Chem.* **2017,** *238*, 667-675.
181. Vandenryt, T.; van Grinsven, B.; Eersels, K.; Cornelis, P.; Kholwadia, S.; Cleij, T. J.; Thoelen, R.; De Ceuninck, W.; Peeters, M.; Wagner, P., Single-Shot Detection of Neurotransmitters in Whole-Blood Samples by Means of the Heat-Transfer Method in Combination with Synthetic Receptors. *Sensors* **2017,** *17*, 2701.
182. Ran, G.; Chen, X.; Xia, Y., Electrochemical Detection of Serotonin Based on a Poly(Bromocresol Green) Film and Fe3O4 Nanoparticles in a Chitosan Matrix. *RSC Adv.* **2017,** *7*, 1847-1851.
183. Revin, S. B.; John, S. A., Electrochemical Sensor for Neurotransmitters at Physiological pH using a Heterocyclic Conducting Polymer Modified Electrode. *Analyst* **2012,** *137*, 209-215.
184. Charlier, J. C., Defects in Carbon Nanotubes. *Acc. Chem. Res.* **2002,** *35*, 1063-1069.
185. Rubio-Giménez, V.; Galbiati, M.; Castells-Gil, J.; Almora-Barrios, N.; Navarro-Sánchez, J.; Escorcia-Ariza, G.; Mattera, M.; Arnold, T.; Rawle, J.; Tatay, S.; Coronado, E.; Martí-Gastaldo, C., Bottom-Up Fabrication of Semiconductive Metal-Organic Framework Ultrathin Films. *Adv. Mater.* **2018,** *30*, 1704291.
186. Foster, M. E.; Sohlberg, K.; Allendorf, M. D.; Talin, A. A., Unraveling the Semiconducting/Metallic Discrepancy in $Ni_3(HITP)_2$. *J. Phys. Chem. Lett.* **2018,** *9*, 481-486.
187. Nagabooshanam, S.; Roy, S.; Mathur, A.; Mukherjee, I.; Krishnamurthy, S.; Bharadwaj, L. M., Electrochemical Micro Analytical Device Interfaced with Portable Potentiostat for Rapid Detection of Chlorpyrifos using Acetylcholinesterase Conjugated Metal Organic Framework using Internet of Things. *Sci. Rep.* **2019,** *9*, 19862.
188. Ross, A. E.; Venton, B. J., Nafion-CNT Coated Carbon-Fiber Microelectrodes for Enhanced Detection of Adenosine. *Analyst* **2012,** *137*, 3045-3051.
189. Li, C.-M.; Zha, Q.-X., Electrodes Surface-Intercalated with Powder Catalysts: II. Microelectrodes Surface-Intercalated with Powder Catalysts. *Acta Chim. Sinica* **1988,** *6*, 14-20.
190. Kim, G. H.; Kim, K.; Lee, E.; An, T.; Choi, W.; Lim, G.; Shin, J. H., Recent Progress on Microelectrodes in Neural Interfaces. *Materials* **2018,** *11*, 1995.
191. Wei, W.; Song, Y.; Wang, L.; Zhang, S.; Luo, J.; Xu, S.; Cai, X., An Implantable Microelectrode Array for Simultaneous L-Glutamate and Electrophysiological Recordings In Vivo. *Microsyst. Nanoeng.* **2015,** *1*, 1-6.

For table of contents only.